Emergent mystery in the Kondo insulator samarium hexaboride

Lu Li ✉, *Kai Sun*, *Cagliyan Kurdak and J. W. Allen*

Abstract | Samarium hexaboride (SmB_6) is an example of a Kondo insulator, in which strong electron correlations cause a band gap to open. SmB_6 hosts both a bulk insulating state and a conductive surface state. Within a Fermi-liquid framework, the strongly correlated ground-state electronic structure can be mapped to a simple state resembling a topological insulator. Although uncertainties remain, many experiments provide compelling evidence that the conductive surface states have a topological origin. However, the bulk behaviour is less well understood and some experiments indicate bulk in-gap states. This has inspired the development of many theories that predict the emergence of new bulk quantum phases beyond Landau's Fermi-liquid model. We review the current progress on understanding both the surface and the bulk states, especially the experimental evidence for each. A mystery centres on the existence of the bulk in-gap states and why they appear in some experiments but not others. Adding to the mystery is why quantum oscillations in SmB_6 appear only in magnetization but not in resistivity. We conclude by elaborating on three questions: why SmB_6 is worth studying, what can be done to move forwards and what other correlated insulators could give additional insight.

Topological insulators (TIs) represent the triumph of single-electron band theory[1,2], whereas strongly correlated electron physics describes phenomena such as the Kondo effect and high-temperature superconductivity. The convergence of TIs and strongly correlated physics leads to new phenomena, as in the case of the Kondo insulator samarium hexaboride (SmB_6).

SmB_6 is a widely studied, strongly correlated material. In SmB_6, though its activation energy is no more than 5 meV, the bulk resistivity increases by more than 100,000 times as the temperature decreases from 300 K to 3 K. Kondo insulators involve compounds containing rare-earth elements where *f*-shell electrons generally provide a localized magnetic moment and a strong interaction[3,4]. The hybridization between itinerant electrons and localized orbitals opens a gap and makes the material insulating[3]. In certain Kondo insulators such as SmB_6, the ground-state electronic structure in the strongly correlated system can be mapped to a simple electronic state that resembles a TI (REFS[5,6]). As a result, in the ground state of the Kondo insulator, there exists a bulk insulating state and a conductive surface state[7–9]. 2D devices based on Kondo insulators would realize topologically protected surface conduction while maintaining a completely insulating bulk state. Many experiments, ranging from photoemission, tunnelling spectra to quantum oscillations, provide compelling evidence for the existence of the surface state[10–13]. The material is further applied to build a highly effective spintronic device[14,15].

Conversely, if the gap does not open exactly as expected in the *f*–*d* hybridization picture, various bulk in-gap states may exist in the insulating gap of SmB_6. Some experiments indicate the existence of such in-gap states[16]. Such an exotic state leads to a number of open questions, such as why quantum oscillations appear only in magnetization and if quantum oscillations reveal an unconventional bulk insulator. These inspired the development of many theories, predicting that new quantum phases with striking exotic physics properties may have emerged in this material[17–21].

In this Review, we provide a brief discussion of the theory and material-growth considerations of SmB_6. The focus of this Review is the analysis of various transport, photoemission and quantum-oscillations experiments that have been done on this material. The numerous studies provide a great deal of often confusing and/or contradictory information, and we bring together common threads that may provide a coherent understanding of the data. In particular, we urge the community to elucidate the impact of particular sample-growth and preparation processes on its properties. We conclude by asking a series of outstanding questions, including how correlated the surface states of SmB_6 are. This question arises from the effective mass differences and may help us to understand the mystery of SmB_6.

Department of Physics, University of Michigan, Ann Arbor, MI, USA.

✉*e-mail: luli@umich.edu*

https://doi.org/10.1038/s42254-020-0210-8

Key points

- The Kondo insulator samarium hexaboride (SmB_6) is a perfect insulator owing to strong electronic correlations. It is the first experimentally confirmed example of a strongly correlated topological material.
- The topological band structure and the consequent metallic surface states are determined and protected by the crystal point symmetry in SmB_6. The universal topological predictions are confirmed by spin-resolved and angle-resolved photoemission spectroscopy, although some unresolved issues remain.
- Surface electrical transport is established in SmB_6. Spin-dependent experiments both confirm basic topological predictions and indicate the potential for spin-based electronic applications.
- There is a mystery as to whether Landau-level quantum oscillations in SmB_6 have a bulk or surface-state origin, and why they appear only in magnetization.
- The mystery calls for a new growth method for SmB_6, a broad search for other strongly correlated topological materials and further detailed theoretical pictures for the possible ground states of mixed-valent materials.

Theory

In SmB_6, the Sm atoms form a simple cubic lattice, whereas the B atoms fill in between. At low energy, electronic excitations in SmB_6 are largely composed of the *f*-state and *d*-state of the Sm atoms, hybridized with some boron states. In contrast to conventional metals or semiconductors, where interactions between electrons are weak and can often be treated as a perturbation effect, in SmB_6, electrons on the *f*-states couple very strongly with one another. The presence of such strong electron–electron interactions grants SmB_6 intriguing physical properties in sharp contrast to conventional metals or semiconductors, such as a huge electron effective mass that is orders of magnitude higher than that of free electrons. To emphasize the highly non-trivial impacts of the strong electron–electron interactions, also known as strong correlations or strong coupling, materials like SmB_6 are often referred to as strongly correlated materials, whereas conventional metals and semiconductors are known as weakly correlated.

Although a naive valence counting predicts a mixed-valence metal, at low temperature, strong interactions between *f*-electrons open up an energy gap, transforming the material into an insulator with a small energy gap on the meV scale. Owing to its strong coupling nature, which makes it a challenge to develop controlled theoretical treatment, the precise microscopic origin of this gap remains an open question. However, at the macroscopic level, the crystalline structure enforces strong symmetry constraints on this material. As will be explained below, these constraints allow only two possible scenarios: SmB_6 is either a TI or an exotic insulator beyond the Fermi-liquid description of Landau.

SmB_6 as a TI. If the band-structure theory and Landau's Fermi-liquid theory correctly capture the low-energy physics of SmB_6, the topological properties of this material can be deduced based on its band structure. For SmB_6, due to the strong coupling of the *f*-electrons, as well as their narrow bandwidth and small energy gap, resolving the details about the band structure (especially for the strongly correlated *f*-bands) remains a theoretical and experimental challenge. However, the physics at high-symmetry points (with momentum $k = 0$ or π) are very well understood, and it turns out that this information alone is already sufficient to dictate the topological indices and qualitative features of the topological surface states.

As illustrated in FIG. 1a, at low temperature, there are three *f*-bands and one *d*-band near the Fermi energy, with red (blue) indicating that the band is mostly composed of *d*-states (*f*-states) of the Sm atom. The *d*-band is less correlated and, so, is well understood. Its energy is above the Fermi level E_F at all high-symmetry points except the X points (momentum points (0,0,π), (0,π,0) or (π,0,0), marked by the blue dots in FIG. 1b), where the band is below E_F. The three *f*-bands are below the Fermi level for all high-symmetry points except X. At X, if the insulating behaviour of SmB_6 is due to a band gap, one of the three *f*-bands must be pushed to above E_F, in order to open up an insulating gap. In other words, a band inversion between an *f*-band and a *d*-band takes place at each X point. These energy bands can be classified according to their symmetry, following space group and point group[22]. Among these two inverted bands, the less-correlated *d*-band is known to belong to the Γ_7^+ representation of the D_{4h} point group at X. The more strongly correlated *f*-bands are less understood owing to their strong coupling nature. However, to open up a band gap, the point-group and/or space-group symmetry requires that the inverted *f*-band must belong to the Γ_7^- representation at X, because, otherwise, the space-group compatibility relation will prohibit the formation of a full gap, resulting in a nodal semimetal instead of an insulator.

In the study of topological states of matter, it has long been known that band inversions between energy bands with different symmetry play a crucial role. Recently, theoretical frameworks, such as topological quantum chemistry and symmetry indicators, provide a systematic classification of potential topology in non-magnetic materials[23–30]. For SmB_6, thanks to its O_h point group symmetry, the *f*–*d* band inversion at X is sufficient to fully dictate its topology. In particular, using techniques developed for topological band insulators[31,32], it can be shown that the symmetry of these two bands (Γ_7^+ and Γ_7^-) pins the values of two topological indices: the Z_2 topological index of TIs and the mirror Chern number of topological crystalline insulators (up to modulo *n* for mirror planes with *n*-fold rotational symmetries)[33].

Furthermore, these two indices dictate the topological surface states of SmB_6. On each 2D surface of SmB_6, a Brillouin zone (BZ) can be defined. Depending on the surface orientation, the surface BZ takes different shapes and symmetry, as shown in FIG. 1b, where we project the bulk BZ onto various surfaces. To distinguish bulk and surface BZs, following the standard convention, an overbar is used to label surface momentum points in the surface BZ. As illustrated in FIG. 1c–e, for (100) and (111) surfaces, the number of locations of the surface Dirac cones are fully dictated. For the (110) surface, the topology allows two possible surface states, as shown in FIG. 1d. Although seemingly different, these two options are, in fact, topologically equivalent and can be adiabatically deformed into each other. It should be highlighted that, in the left panel of FIG. 1d, the $\overline{X}$ point has

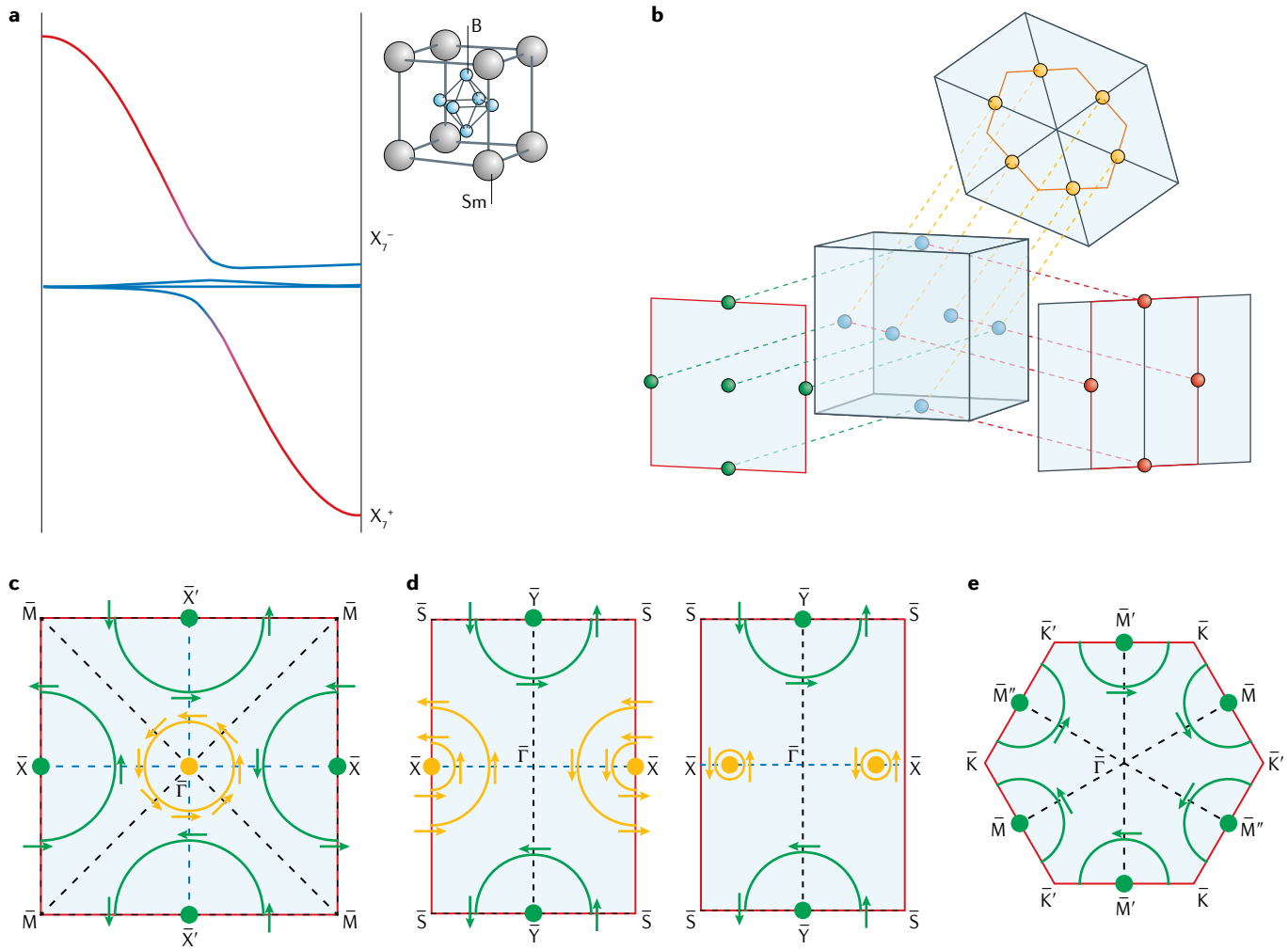

Fig. 1 | **Schematic bulk band structure and topological surface states of SmB_6. a** | Schematic band structures for bands near the Fermi energy. The red (blue) colour here indicates that the band is mostly composed of *d*-states (*f*-states) of Sm. At each band-inversion point X, a band inversion occurs between an *f*-band and a *d*-band with symmetry representations Γ_7^- and Γ_7^+, respectively. The inset shows the crystal structure of SmB_6, where big (small) spheres represent Sm (B) atoms. **b** | The projection of bulk band inversion points to the (100), (110) and (111) surfaces. The cube marks the bulk Brillouin zone, and the three band-inversion points (X) are marked by blue dots. The dashed lines demonstrate projection of bulk band-inversion points onto various surfaces and the red lines indicate the surface Brillouin zones. **c**–**e** | Topological surface states on the (100), (110) and (111) surfaces, respectively. The ochre discs and green circles represent surface Dirac points and Fermi surfaces from these Dirac cones, respectively. The spin structure for each Fermi surface is marked by the arrows. The dashed lines are the projection of bulk mirror planes. The colour of a dashed line represents the mirror Chern number $C^{\pm}$ of the corresponding bulk mirror plane, where black and blue lines imply $C^{\pm} = 1$ and $C^{\pm} = 2$, respectively.

two Dirac points, which results in two concentric Fermi surfaces (FSs) around $\bar{X}$. Other discs in FIG. 1c–e represent a single Dirac point each. As can be seen from these figures, all surfaces contain an odd number of surface Dirac cones, consistent with the theory expectation of a 3D strong TI. In FIG. 1c–e, the dashed lines are the projection of bulk mirror planes. The colour of a dashed line represents the mirror Chern number $C^{\pm}$ of the corresponding bulk mirror plane, where black and blue imply $C^{\pm} = 1$ and $C^{\pm} = 2$, respectively (modulo n). According to the topological bulk-edge correspondence, $C^{\pm}$ gives the number of Dirac cones that should be located along this line, and, thus, on each black (blue) dashed line, there should exist one (two) Dirac cone(s). To satisfy this constraint for all mirror planes (dashed lines), the surface states must organize into the patterns shown in FIG. 1c–e.

In contrast to the number and locations of the surface Dirac cones, which are fully dictated by the topology, the spin textures of the surface states are more involved and can reveal information about microscopic properties[34–36], such as crystal-field splittings, correlation effects and surface conditions. In general, topology and symmetry enforce two constraints. Firstly, spins around any Dirac cones must exhibit a non-trivial winding and, secondly, to preserve the mirror symmetry, the fermion spin on a mirror plane (represented by the dashed lines in FIG. 1c–e) must be perpendicular to the plane. However, these two constraints do not fully determine the spin texture. For example, (some or all of) the arrows in FIG. 1c–e

can be flipped without violating these constraints. Topology cannot fully determine a universal spin texture because topological indices (for example, mirror Chern numbers) directly dictate pseudo spins instead of physical spins, which are measured in experiments like spin-resolved and angle-resolved photoemission spectroscopy (ARPES). For example, on mirror planes, both pseudo spins and physical spins are expected to be perpendicular to the mirror plane, but they may align or anti-align with each other, depending on the orbital composition of the wavefunctions. To translate between pseudo spins and physical spins requires a combined effort from theoretical, numerical and experimental studies. Theoretically, it has been found that the winding structure is highly sensitive to crystal-field splittings[34–36], and, thus, the spin texture of the surface states may potentially provide a new experimental tool to probe crystal-field effects through topological surface states. On the numerical side, in addition to band structures and topological indices, first-principle and dynamical mean-field theory studies can also provide valuable insights about this mapping between pseudo spins and physical spins[37–44].

Beyond Landau's Fermi-liquid theory. It is worthwhile to emphasize that the analysis above, regarding topology and surface states, although universal and independent of the microscopic details, is based on the assumption that the insulating behaviour of SmB_6 is due to a band gap. If this assumption fails in SmB_6, it leads to the possibility of exotic insulators beyond Landau's Fermi-liquid theory. In direct contrast to a band gap, which gaps out both charged and charge-neutral degrees of freedom in the bulk, an exotic correlated insulator may only have a charge gap, whereas charge-neutral degrees of freedom remain gapless and may even exhibit Fermi-surface-like behaviour. Such possibilities have become a new frontier in the study of SmB_6 and related materials, such as YbB_{12}, where new theoretical ideas[17–21,45–47] and experimental investigations[16,48–50] are actively explored. For SmB_6, the existing knowledge about possible charge-neutral excitations beyond Landau's theory is still incomplete and some fundamental questions still need to be answered, such as whether the charge-neutral degrees of freedom originate from *d*-electrons or *f*-electrons. The conventional wisdom hints at the more strongly correlated *f*-electrons, whereas certain experimental observations, such as the spin excitations from neutron scattering[51] and the light effective mass reported in quantum-oscillation studies[10,16], indicates that the *d*-electrons might play a very important role. Despite the limited knowledge, one thing is certain about this scenario: exotic phenomena beyond fundamental doctrines, such as Landau's adiabatic path between the interacting Fermi liquid and the non-interacting Fermi gas, shall emerge.

Finally, these two scenarios are not necessarily mutually exclusive, and it remains an interesting open question whether both scenarios can coexist in the same material, either simultaneously or as two competing ground states stabilized in different parts of the phase diagram. Simultaneous existence would lead to a new quantum state that exhibits both topological surface states of topological band insulators and non-trivial bulk quasiparticle excitations beyond the theory of Landau. The existence of competing ground states would imply a quantum/classical phase transition between a topological band insulator and a correlated insulator. In particular, considering that, as will be discussed below, current experiments suggest that certain physical properties of SmB_6 might be sensitive to the growing methods of the material, the possibility of two competing ground states might offer a clue for understanding their physical origin.

Materials considerations

It is important to be aware of certain materials considerations for experiments on SmB_6. First, there are two general methods to grow SmB_6 single crystals. The melting point of SmB_6 is extremely high (about 2,400 °C). The flux method[52] dissolves SmB_6 polycrystalline powders into aluminium flux at lower temperatures (~1,450 °C) and this mixture is cooled down, during which the naturally generated temperature gradient crystallizes SmB_6. By contrast, the float-zone method raises the growth temperature high enough to melt the SmB_6 polycrystalline rod to start the crystallization[53]. Both growth methods generate SmB_6 of the same structure, yet, some experimental results appear to depend on which type of sample is studied. We will revisit this in the final section.

Second, for crystals grown by either method, the (100) surface most readily obtained for this cubic crystal, and, therefore, most frequently studied, is polar. An ideal surface would be terminated either as B or Sm, but scanning tunnelling microscopy (STM) studies by many groups[11,54–61] have revealed that actual cleaved surfaces display domains with a variety of B and Sm morphologies, and that pure Sm domains manifest a 1×2 reconstruction. Perhaps related, spectra changing with time after initial surface preparation have been reported in various measurements[62–65]. The morphological effects appear to depend not only on the detailed circumstances of the cleave but also on the growth method of the crystal. Furthermore, different morphologies manifest different electronic structures in the tunnelling spectra taken during the STM studies. How all these (100) cleave issues impact other surface-sensitive measurements has been difficult to fully characterize and understand. For example, morphology domain sizes observed in STM are typically much smaller than can be probed in ARPES, although it has been reported[61] that cleaved (100) surfaces of float-zone samples can be terminated exclusively with B or Sm. Finally, it is not at all clear to what extent these vacuum-cleaved surface-termination subtleties in spectroscopy are important for transport measurements discussed in the next section, since these measurements are made on crystals with buried interfaces below a thin surface-oxidation layer.

Transport properties

The electrical properties of SmB_6 have been studied as a mixed-valent material for five decades[4,66–69]. A typical temperature-dependent resistivity trace of SmB_6 is shown in FIG. 2a. At room temperature, the material appeared

1×2 reconstruction
The freedom from complete bulk coordination can allow surface atoms to spontaneously 'reconstruct' to take atomic positions altered from the perfect surface termination of the bulk. In a '1×2' or '2×1' reconstruction, the alteration doubles the length of one of the two translation vectors of the surface unit cell, which halves the surface Brillouin zone in one direction. For the cubic crystal SmB_6, this halving has the effect of rendering the $\overline{\Gamma}$ and the $\overline{X}$ points of the un-reconstructed surface Brillouin zone to be equivalent.

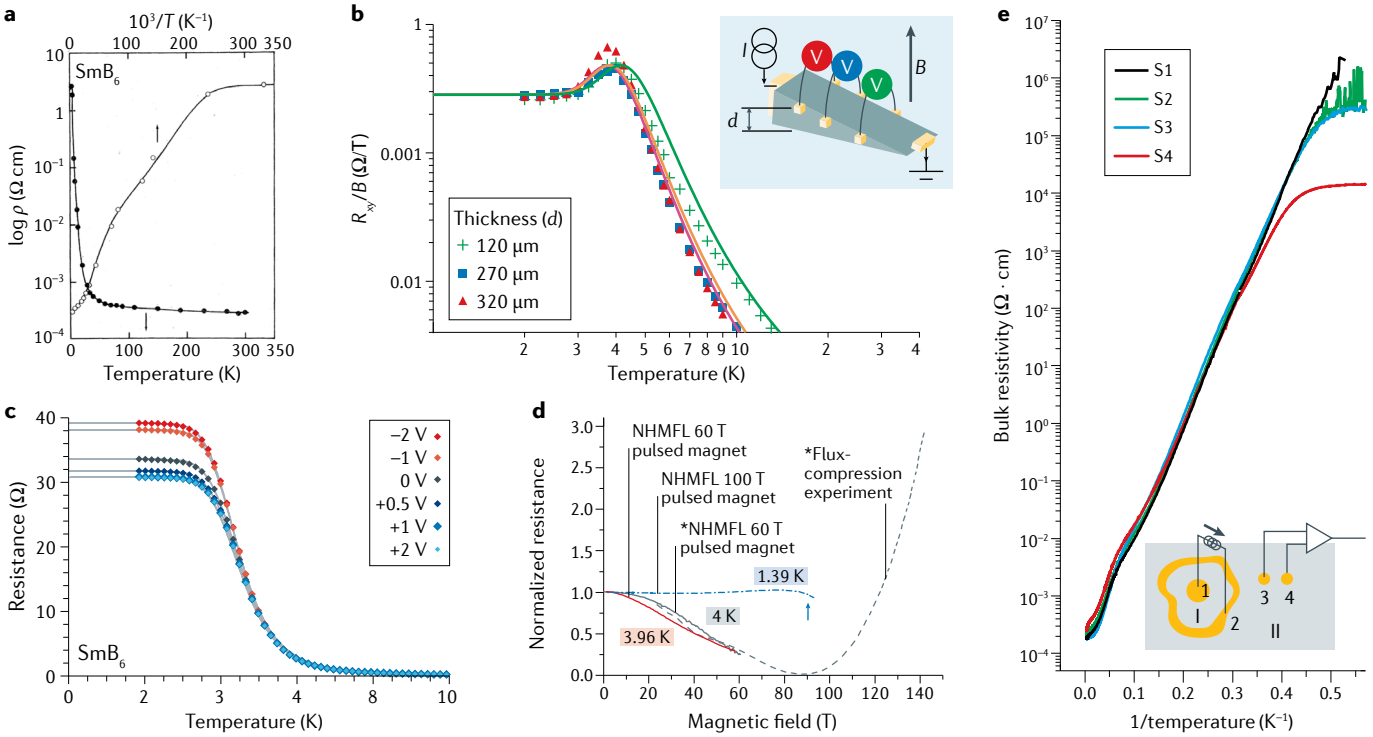

Fig. 2 | **Transport characterization of SmB_6. a** | Temperature dependence of the resistivity of SmB_6. **b** | Hall resistance divided by the magnetic field (R_{xy}/B) versus temperature, T, at three different thicknesses in a wedge-shaped sample. A schematic diagram of the transport structure is illustrated as an inset. The Hall resistivity at low temperatures appears to be independent of the sample thickness, indicating that transport is due to surface charges. **c** | The temperature-dependent electrical resistance of SmB_6 for different ionic-gate voltages obtained from a four-terminal Corbino sample fabricated on the (001) surface. The ionic liquid covers the whole sample and the gating only affects the low-temperature resistance plateau. **d** | Magnetoresistance traces of a two-terminal Corbino sample obtained using pulsed-field measurements at 1.39 K and 3.96 K. The data are plotted together with earlier magnetoresistance traces from REF.[102] denoted by asterisks, including the highest field data obtained by using an explosively driven flux-compression system. The data are all in agreement with each other. The hybridization gap is expected to close at a magnetic field above 100 T. The magnetoresistance traces do not show Shubnikov–de Haas oscillations. **e** | Bulk resistivity of SmB_6 grown stoichiometrically (S1) and non-stoichiometrically (S2–S4) as a function of inverse temperature. Sample S1 was grown using the Al flux method, where Sm and B were added to Al with the expected stoichiometry of 1 to 6. For the growth of samples S2, S3 and S4, the portion of Sm was reduced by 10%, 25% and 40%, respectively. The data are obtained by combining standard resistivity measurements with an inverted resistance measurement, which allows us to access bulk resistivity of a topological insulator, even in a regime where the transport is dominated by surface conduction. The activated behaviour extends over ten orders of magnitude, a remarkable finding suggesting that the transport gap might be protected against disorder in this material. The inset shows a schematic diagram of inverted resistance measurement, which consists of a current lead fully enclosing the other current lead and two voltage leads placed outside the loop. NHMFL, National High Magnetic Field Laboratory. Panel **a** adapted with permission from REF.[68], ACS. Panel **b** adapted from REF.[9], Springer Nature Limited. Panel **c** adapted with permission from REF.[102], APS. Panel **d** adapted with permission from REF.[103], APS. Panel **e** adapted with permission from REF.[109], PNAS.

to be a reasonably good conductor with a resistivity that is about two orders of magnitude larger than silver or gold. The conduction is mainly due to *d*-electrons. The *f*-electrons, which are also present at the Fermi energy of the material, act as strong skew-scattering centres[70], leading to a positive Hall coefficient[68,71–74] and very low electron mobility at high temperatures[74]. Even though the activated behaviour of the resistivity was known for more than 50 years[4,66,67], the strongest evidence for the insulating behaviour came from the Hall measurements[68], indicating that the carrier density was also activated with a similar activation energy, suggesting that the material had a cryogenic gap arising from the hybridization of *d*-electrons and *f*-electrons[75–77]. Furthermore, optical[78,79], photoemission[80,81] and tunnelling[8,82] spectroscopy measurements also indicate the presence of a gap, consistent with the activated behaviour obtained from transport measurements.

Surface states. Unlike ordinary insulators, the resistivity of SmB_6 is found to saturate at low temperatures ($T < 4$ K). All the transport features, including the activated behaviour and the cryogenic resistance plateau, appeared to be robust among different samples. In the early years prior to the theory suggestion of the TI ground state, it was assumed that the transport must be dominated by bulk carriers. However, within the bulk conduction hypothesis, it was difficult to come up with a well-accepted explanation for the residual resistivity, which remained a mystery after more than 30 years. The solution to this mystery came from the theoretical prediction[5] that SmB_6 is a correlated TI. In the TI description, SmB_6 must harbour topologically protected metallic surface states that would give rise to the residual low-temperature resistivity and all the difficulties with fundamental resistivity limits described above for 3D bulk explanations would be evaded.

The presence of surface conductivity in SmB_6 was first demonstrated by three independent measurements from different research groups. First, a non-local transport experiment using a double-sided device structure allowing a variety of non-local transport measurements that put different emphases on bulk and surface conductivities of this material[7]. Second, Hall measurements performed on a wedge-shaped sample with multiple contacts[9]. Finally, point-contact spectroscopy measurements[8]. In the wedge-shaped sample shown in FIG. 2b, the Hall resistivity is found to be independent of the sample thickness at low temperatures consistent with surface transport. Furthermore, the angle-dependent magnetotransport measurements performed by multiple groups[83–85], studies on ion-irradiated samples[86] and transport measurements performed on samples with different thicknesses also indicated the presence of a surface conducting layer, but did not reveal their topological nature.

One of the predictions of the topological hypothesis is that there should be quantum corrections to conductivity leading to weak antilocalization[87,88]. Weak-antilocalization corrections have been measured by two groups[89,90], providing further support for the topological nature of the surface states. Similar transport experiments did not exhibit weak-antilocalization features; instead, hysteretic behaviour in low-field magnetoresistance traces were found to be dependent on the magnetic sweep rate, suggesting that this behaviour must be due to extrinsic magnetic-field effects, such as the magnetocaloric effect or glassy ordering in the native surface oxide[85]. Other transport experiments have also been performed to probe the helical spin structure of surface electrons in this material. Most significantly, there is a recent report of a clear spin signal on the surface of SmB_6 through the inverse Edelstein effect[14] and using specially designed transport geometries with ferromagnetic contacts[91–93]. Furthermore, there is a report of perfect Andreev reflection in a superconductor point-contact-spectroscopy experiment on SmB_6, which supports spin-momentum locking of surface electrons in SmB_6 (REF.[94]). Given the potential spintronic applications of SmB_6, new thin-film growth methods have also been developing[95–99].

Note that, despite numerous transport studies, the full electrical characterization of surface conduction in SmB_6 turned out to be more challenging than expected for two reasons. Firstly, the surface of SmB_6 hosts three Dirac cones, requiring a multi-pocket transport model. Secondly, it is found that the surface conduction is typically polluted by conduction through transport through subsurface cracks, especially in samples with roughly polished surfaces[100,101]. The first rough estimates for carrier density and mobility came from Corbino structures focusing on individual surfaces. For example, temperature-dependent electrical-resistance traces obtained from a Corbino sample for different ionic-gate voltages are shown in FIG. 2c. The analysis revealed a field-effect mobility of 133 $cm^2 (V s)^{-1}$ and a large carrier density of ~2×10^{14} cm^{-2} for the (100) surface of SmB_6 (REF.[102]), which appeared to agree with the effective parameters extracted from angle-dependent magnetoresistance measurements[85]. Many groups have also tried to characterize the surface layer by searching for Shubnikov–de Haas oscillations at high magnetic fields[103]. One such magnetoresistance trace is shown in FIG. 2d. Unfortunately, even at magnetic fields as high as 90 T, such oscillations were not observed, which was consistent with the mobility estimates coming from Corbino samples. The Hall measurements gave unphysically large carrier densities[68,69], most likely due to the presence of parallel conduction paths through subsurface cracks. Recently, instead of relying on Hall measurements, a study analysed the angle-dependent magnetoresistance measurements on finely polished Corbino samples together with the carrier densities reported from ARPES measurements and determined electron mobilities ranging from 148 to 168 $cm^2 (V s)^{-1}$ for electrons occupying the smaller Γ-pocket and mobilities ranging from 4.8 to 9.2 $cm^2 (V s)^{-1}$ for electrons occupying the larger X-pockets[101]. The exact values of these parameters are still under debate, as there are significant disagreements between parameters extracted from transport, scanning tunnelling and magneto-torque quantum-oscillations measurements.

Bulk states. In addition to the study of surface conduction, there has been renewed interest in the study of the bulk properties of SmB_6, especially following the report of quantum oscillations in magnetization coming from an unconventional bulk FS in this material[10,16]. This experiment required a fresh look at the underlying physics of gap formation and emerging theories that focus on the bulk of SmB_6. On the experimental side, point-contact spectroscopy and high-frequency-transport measurements have been used to study both the opening of the gap as a function of temperature and states that may be present within the gap. The closure of the transport gap has also been studied using high-pressure[69,104] and high-magnetic-field measurements[103,105]. The microscopic mechanism for this experimental observation still remains unclear and needs further investigations. Here, we report the observation to highlight the fact that the material remains an insulator (with a non-zero gap) for the field strength applied in quantum-oscillation experiments. Furthermore, it is possible to go from an insulating to a conducting state by introducing a high concentration of substitutional atoms[106].

Owing to the symmetry-protection nature of TIs, magnetically doped samples such as Gd-doped SmB_6 have been particularly interesting, as the presence of magnetic dopants breaks a key ingredient of TIs and topological surface states[107], which is the time-reversal symmetry. The electrical properties of the bulk have also been studied using a new type of transport measurement, called 'inverted resistance measurements' (REF.[108]), which means that surface conduction can be bypassed and bulk resistivity can be measured. From room temperature to 4 K, the bulk resistivity changes by five orders of magnitude; it changes by another five orders of magnitude from 4 K to 2 K (REF.[109]). The bulk resistivities obtained using this method on samples that were grown with different stoichiometries are shown in FIG. 2e. There are two remarkable features in these data. First, the bulk d.c. resistivity rises by a factor of 10^{10} on

Weak antilocalization
A quantum correction to conductance arising from quantum-interference effects in materials with strong spin–orbit interaction.

Edelstein effect
Accumulation of transverse spin due to the flow of an electric current in a thin film or a two-dimensional material with a strong spin–orbit interaction.

Corbino structures
A transport geometry with concentric circular contacts used to measure the electrical conductivity of a material.

Shubnikov–de Haas oscillations
Oscillations observed in transport measurements performed on conductors as a function of magnetic field. The oscillations arise from the formation of Landau levels separated from each other by the cyclotron energy.

Γ-pocket
Fermi-surface pockets refer to the location of conducting surface electrons or holes in reciprocal space. For the (001) surface, a cubic material with a lattice constant a, the Γ-pocket refers to the surface electrons located around the Γ point, (0,0), and the X-pockets refers to the electrons located around X points, (0,π/a) and (π/a,0).

Off-stoichiometry
Stoichiometry refers to the ratio of different atoms forming a crystal. For a stoichiometric material, the ratio is described by a fraction of natural numbers (i.e. 1:6 in the case of SmB_6). Off-stoichiometry is a measure of disorder, where the ratio of constituent atoms deviates from the expected fraction of natural numbers.

cooling from 300 K to 2 K, with a well-defined activation energy of 4.0 meV. Second, the activated behaviour appears to be the same in samples prepared with large samarium-to-boron off-stoichiometry. In other words, the bulk of SmB_6 is truly insulating and appears to be immune to disorder[109].

This property is quite different from standard TIs like Bi_2Se_3, where the addition of impurities creates in-gap hydrogenic bulk states, which typically result in an unwanted bulk conduction channel. The existence of these shallow hydrogenic impurity states relies on the effective mass approximation, an assumption that is not justified in SmB_6 (REF.[110]), which suggests that the gap protection and immunity against disorder must be intrinsic properties of this material. Perhaps, similar to the Bardeen–Cooper–Schrieffer mechanism[111], the gap formation in SmB_6 occurs in such a way that the gap is insensitive to defects. There is a recent alternative theory dealing with disorder in mixed-valent insulators such as SmB_6 (REFS[112,113]). It suggests that, after the opening of the hybridization gap, the conduction band would have a Mexican-hat-type dispersion, which would support an unusual bulk hydrogenic impurity band. In this theory, the critical density does not depend on the Bohr radius of the hydrogenic levels but is, instead, determined by the radius of the Mexican-hat dispersion in k-space, and, thus, this new theory has the possibility of explaining the robustness of the insulating behaviour at low impurity concentrations, together with known differences between d.c. and a.c. conductivities[49].

ARPES

If certain experimental and theoretical requirements can be met[114,115], photoemission spectroscopy measures the single-particle spectral function for removing an electron with binding energy E, here taken as measured relative to the Fermi energy E_F. ARPES then yields the spectral function $A(\boldsymbol{k},E)$, with $\boldsymbol{k}$ being the crystal momentum. ARPES studies have acquired an almost defining status for studying TI materials because $A(\boldsymbol{k},E)$ is generally fundamental for electronic structure, and ARPES is very surface sensitive, making it particularly useful for identifying TI surface states[1]. In an ARPES experiment, photons of known energy are shone on a surface and the angle and kinetic energy of photoemitted electrons are detected[114]. In the photoemission process, the momentum component parallel to the surface is conserved, but the perpendicular component k_z changes by an amount that depends on the surface potential. Using the ansatz[116] of an 'inner potential', V_0, kinematic relations can be derived whereby both the parallel and perpendicular components of the photohole momentum can be deduced, using the photon energy and the photoelectron kinetic energy and emission angle, which are measured in the experiment. For fixed photon energy, the photohole momentum varies with emission angle on a spherical surface in $\boldsymbol{k}$-space, and the k_z value for normal emission is the radius of this spherical surface. The k_z value varies with photon energy in a way that depends quantitatively on the empirically determined[116] and material-dependent V_0 parameter, as shown specifically for SmB_6 in FIG. 1 of REF.[117].

The analyser angle and energy resolution, and also the photon-energy resolution, determine the precision with which the parallel momentum and the binding energy E can be determined. It can be shown[118] that the photoelectron lifetime induces uncertainty (broadening) in k_z. In spin-resolved ARPES (SARPES), the photoelectron spin is also detected, from which the photohole spin can be known. Of the many SmB_6 photoemission studies over the years, we only refer to those since 2012 (REFS[12,39,61–63,65,81,117,119–136]). Photoemission overviews can be found in REFS[137–139]. Our overview draws on a subset of studies (referenced in the figure captions) to present the most recent and/or the most basic aspects of low-temperature ARPES and SARPES. We have chosen not to include temperature-dependent studies[39,42,44,126,128] and certain other subtleties and nuances too specialized or too speculative for a general review of this length.

ARPES studies of SmB_6. Wide-energy-scale ARPES spectra of SmB_6 (REF.[117]) show both band-like dispersing states and atomic-like states with very weak or no dispersion. The dispersing features are bands originating from Sm 5*d* states and B 2*p* states. The 5*d* conduction band, which band calculations show to also have a strong 2*p* admixture, disperses towards E_F between Γ and X from around 1.6 eV below E_F at the X point. The weakly dispersing features are due to electron removal from Sm $4f^6$, resulting in essentially atomic $4f^5$ multiplets, ^6H, ^6F, $^6P_{5/2}$ and $^6P_{7/2}$, located nearest to E_F, and at 1 eV, 3 eV and 3.5 eV below E_F, respectively, and to electron removal from $4f^5$, resulting in atomic $4f^4$ multiplets, ^5I, ^5F, ^5G and ^5D, in the energy range 7 eV to 12 eV below E_F. The observation of such detailed atomic-multiplet structures for both $4f^5$ and $4f^4$ shows that Sm is indeed mixed valent in SmB_6 and that the 4*f* states are very strongly correlated. The separation of ≈7 eV between the lowest energy $4f^5$ and the lowest-energy $4f^4$ multiplets is a measure of the very large on-site 4*f* Coulomb repulsion U. In the absence of the Sm 4*f* electron states, the 5*d* band crossing E_F would produce the metallic FS of a simple metal, as has been verified[140] in the non-4*f* electron-isomorphic reference material LaB_6. Due to the mixed valence of the 4*f* states, SmB_6 is instead a strongly correlated insulator, as we describe next.

Mixed valence occurs in spite of the large U and the crystallographic equivalence of all Sm sites. In the absence of hybridization, the lowest-energy electron-removal transition, from $4f^6$ to $4f^5$, coincides with E_F, so that there is nominally no energy barrier for an electron to move from the 4*f* shell to the conduction band. However, the narrow range spectrum of FIG. 3a, taken on the cleaved surface of a flux-grown sample, shows the $4f^5\,^6H_{5/2}$ state forming the boundary of a nominally 20 meV gap. From the earliest theories[75,76,141] to the more recent[40,42,43], the general understanding of the gap is that it results from hybridization between the 5*d* band and the 4*f* quasiparticle states derived from the $^6H_{5/2}$ multiplet, which, inherently[139], have a one-to-one symmetry correspondence with the six $j = 5/2$ 4*f* bands of the one-electron calculations discussed in the theory section above. Indeed, in FIG. 3a, the $^6H_{5/2}$ state even shows a hint of dispersion, although, thus far, ARPES spectra have not

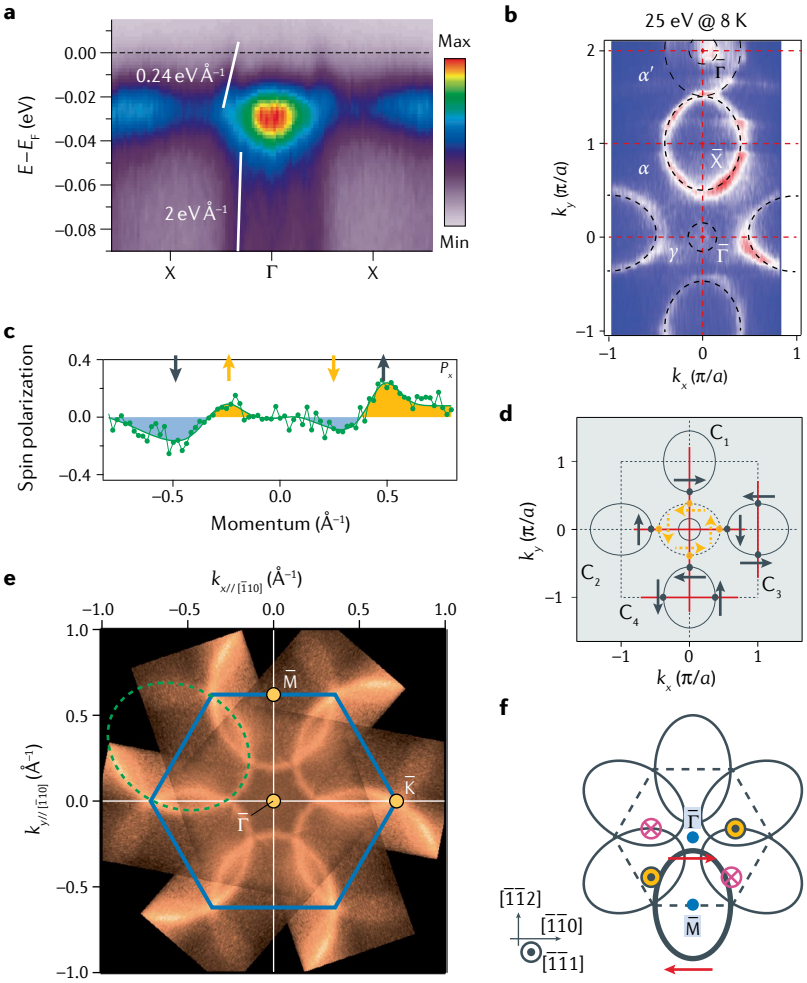

Fig. 3 | **ARPES data on (100) and (111) surfaces, supporting the theory of a topological surface state. a** | Angle-resolved photoemission spectroscopy (ARPES) spectra along Γ–X of the cleaved (100) surface of a flux-grown sample at 6 K with 70 eV photon energy. The conduction band states are rapidly dispersing and $4f^6 \rightarrow 4f^5$ ($^6H_{5/2}$) states are weakly dispersing. The latter states at ≈20 meV form the lower boundary of the bulk gap, which is traversed by in-gap states dispersing to E_F and centred on X and Γ. The white lines show approximate velocities (in eV Å^{-1}) of bulk band and X in-gap states. The in-gap states are k_z-independent (photon-dependent spectra not shown here), indicating surface character. **b** | Fermi surface map of (100) surface of a flux-grown sample at 8 K with 25 eV photon energy, showing in-gap surface-state Fermi surfaces. The oval $\overline{X}$ Fermi surface is strong in the first Brillouin zone and the two $\overline{\Gamma}$ Fermi surfaces are strong in the second Brillouin zone. The large α′ feature was initially assigned as an Umklapp replica of the $\overline{X}$ state, appearing at $\overline{\Gamma}$ only because of a 1 × 2 surface reconstruction, but is, instead, almost certainly an independent state actually centred on $\overline{\Gamma}$, as discussed in the text. **c**,**d** | Spin-resolved ARPES (SARPES) momentum-distribution curves of a cleaved (100) surface of a flux-grown sample taken at 10 meV above E_F, at 20 K with 26 eV photon energy and right circular polarization. Path C_1 has spin polarization only in the *x*-direction, as shown in **c**. Spin texture and ***k***-paths C_1 to C_4 used in SARPES are shown in **d**. The dark arrows show $\overline{X}$ states and the light arrows identify large α′ $\overline{\Gamma}$ state. The number of spin-polarized surfaces per unit cell in **d** is odd, consistent with topological insulator hypothesis. **e** | ARPES E_F map of a (111) surface, at 15 K with 35-eV photon energy and circular polarization, shows surface-state Fermi surface at six $\overline{M}$ points (three per unit cell). Since all $\overline{M}$ points are equivalent, the number of surfaces is an odd number, consistent with topological insulator theory. **f** | The $\overline{M}$ surface-state spin texture from SARPES, analogous to that for the (100) surface in **d**. Panel **a** adapted with permission from REF.[117] *Journal of the Physical Society of Japan*. Panel **b** adapted from REF.[119], CC BY 3.0. Panels **c** and **d** adapted from REF.[124], Springer Nature Limited. Panels **e** and **f** adapted from REF.[136], CC BY 4.0.

resolved the details of the 4*f* dispersion nor shown agreement to any theory. The rapidly dispersing 5*d* conduction band is indicated by a white line showing its velocity of 2 eV Å^{-1} in this region of the spectrum.

TI interpretation of surface states. A band dispersing inside the gap from about 20 meV across E_F can be seen in FIG. 3a. The FS map of FIG. 3b, made by fixing the detector kinetic energy at E_F and varying **k** for the cleaved (100) surface of a flux-grown sample, shows that the band gives rise to an oval electron-like FS centred at $\overline{X}$ points and labelled α. As explained in the summary of the ARPES technique above, the k_z dependence of the band can be measured by varying the photon energy. All such ARPES studies to date[12,119] find, thereby, that its oval FS is k_z-independent, showing it to be a metallic surface state. For this reason, its location in FIG. 3b is given the surface BZ label $\overline{X}$. A TI surface state is predicted for $\overline{X}$ and it fits well with the theory that this feature is very robust, appearing on different cleave-surface terminations[117] and even on aged surfaces[12]. All ARPES studies see this feature and, with one notable exception using 7 eV laser excitation[120], all find essentially the same size FS.

The velocity of the surface state at $\overline{X}$ varies somewhat with ***k*** and data set, but the value of 0.24 eV Å^{-1} shown in FIG. 3a is typical for ARPES studies. Although it is much smaller than that of the bulk conduction band, it is, nonetheless, much larger than might be expected for a strongly correlated bulk gap[42,142]. In the TI theory, the surface-state dispersion to E_F is conical, originating from a Dirac point tip that is below E_F. Such a large velocity implies a small enough cone opening angle that the Dirac point is so far below E_F as to be actually out of the bulk gap, which is unusual but not forbidden in the TI theory. But a major quantitative conflict exists with recent STM quasiparticle interference spectra[60]. These spectra show at $\overline{X}$ a surface state having a much smaller dispersion towards E_F, implying a much larger cone opening angle with the Dirac point tip located close enough to E_F to be inside the bulk gap.

Essential for the TI scenario is that SARPES spectra have shown spin-momentum locking, that is, the spectra are spin polarized in a way that correlates with the momentum ***k***, as shown in FIG. 3c,d. In the experimental procedure, SARPES spectra were taken with circularly polarized incident photons and at fixed binding energy along the four ***k***-contours C_1 to C_4 shown in FIG. 3d. Along each contour, the up and down spin components along the *x*, *y* and *z* directions are measured. The difference between the up and down components, which corresponds to the polarization for each direction, is then determined, as shown for the *x* direction for contour C_1 in FIG. 3c. For this contour, there is no polarization in the *y* or *z* directions. The dark arrows in FIG. 3c point to polarization maxima centred on ***k***-values that correspond to the FS feature at $\overline{X}$. (The light arrows identify maxima at ***k***-values corresponding to the α′ feature in FIG. 3b, centred on $\overline{\Gamma}$ and discussed below.) These SARPES measurements of the gap-filling surface states were very challenging because the energy resolution was 60 meV and the bulk 4*f* states at 20 meV also show a spin dependence[123]. This bulk state spin dependence arises

from photoemission effects when using circularly polarized light[143,144]. To minimize a possible bulk contribution to the spectra, the SARPES 'binding energy' was set at 10 meV above E_F. Also, several other tests were made, for example, it was verified that the surface states show spin polarization when using linearly polarized incident photons, whereas the bulk states do not[123].

Having a TI surface state at $\overline{\Gamma}$ is crucial for the TI theory because there are two $\overline{X}$ points per BZ and the total number of states must be odd. Further examination of FIG. 3a,b does indeed show a small fuzzy feature at the $\overline{\Gamma}$ point, stronger in the second BZ. However, as will be discussed further below, the situation with this small $\overline{\Gamma}$-point feature is generally complicated and there is evidence against a TI origin. In addition, FIG. 3b also shows another larger FS feature centred on $\overline{\Gamma}$, in the second BZ. This is the so-called Umklapp feature, labelled α′ because it is commonly interpreted as actually arising from the original α FS at $\overline{X}$, but appearing at $\overline{\Gamma}$ because of the 2 × 1 surface reconstruction reported for Sm-terminated (100) surfaces in STM studies cited above. However, as is also discussed below, there is very good reason to doubt the Umklapp assignment, and the α′ feature has been proposed[136] as the essential TI surface state intrinsically present at $\overline{\Gamma}$.

Most ARPES studies have been performed on the (100) surface, which is most easily obtained by cleaving. However, in the TI theory, there must be surface states on any surface, and the data in FIG. 3e for the (111) surface prepared on a float-zone sample are particularly compelling[136]. For this surface, TI surface states are predicted for only one surface BZ high-symmetry point, either $\overline{\Gamma}$ or $\overline{M}$ but not both, and not $\overline{K}$. The FS map of FIG. 3e shows FS ovals only for the three equivalent $\overline{M}$ points, which is an odd number, consistent with the TI prediction. That these states are indeed of surface origin was confirmed by a lack of k_z dispersion in photon-energy-dependent spectra[136]. Furthermore, SARPES spectra[136] found the surface states to be spin polarized, as shown in the schematic of FIG. 3f. The set of (111) surface ARPES and SARPES data may be an indication that all the (100) issues discussed next are just distractions away from the central correctness of the TI theory for SmB_6. In particular, it is significant that this surface is non-polar, so that arguments for trivial surface states based on the polar nature of the (100) surface[121], or indeed any surface-specific argument, cannot be used to disprove the TI theory. Also, the simplicity of the (111) TI surface-state counting avoids the counting uncertainty associated with the variability of the (100) surface state at $\overline{\Gamma}$.

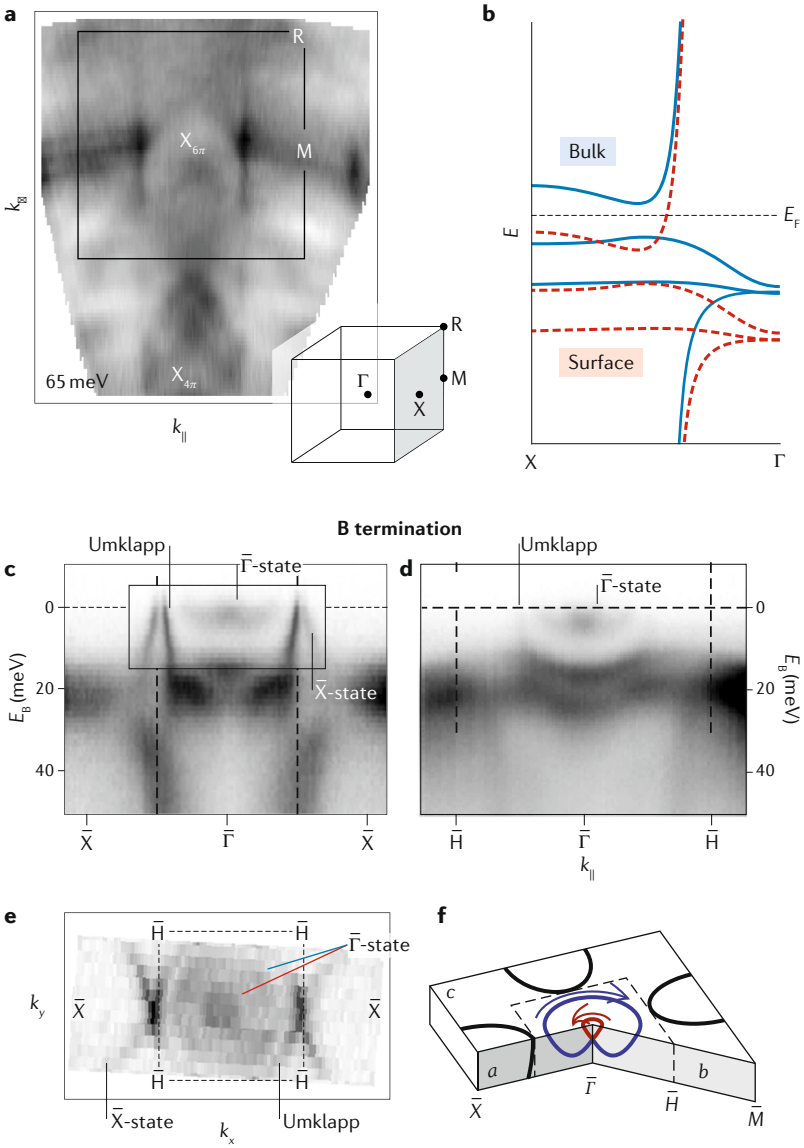

Fig. 4 | **Alternative understanding of SmB_6 (100) surface states, based on ARPES spectra of cleaved float-zone samples. a** | Angle-resolved photoemission spectroscopy (ARPES) photon-energy-dependent map for conduction band at 65 meV binding energy shows not only strong k_z dependence, implying bulk character but also additional k_z-independent streaks, implying 2D surface character. The surface character is understood as the manifestation of a small shift to deeper binding energy of the entire conduction band in the surface layer. **b** | Schematic of alternative scenario of the $\overline{X}$ surface states. There is a surface shift of both band and *f* states to deeper binding energy by an amount larger than the bulk hybridization gap. Thus, the surface gap lies below E_F, which then cuts the surface conduction band above the surface gap and produces the metallic Fermi surface observed in ARPES. **c**,**d** | ARPES spectra along two directions Γ to $\overline{X}$ and Γ to $\overline{H}$, respectively, show distinctly non-topological insulator spin–orbit split Rashba surface state at $\overline{\Gamma}$ for a B-terminated cleave. **e** | E_F map for a B-terminated cleave, showing doubled Fermi surfaces for Rashba surface states at $\overline{\Gamma}$. Also present and labelled are the Fermi surfaces for the surface states at $\overline{X}$ and for the so-called Umklapp feature at $\overline{\Gamma}$, which is almost certainly an independent $\overline{\Gamma}$ state, as proposed in REF.[136] and discussed in the text. **f** | Schematic dispersion and Fermi surface of the Rashba-split state at $\overline{\Gamma}$. All panels adapted from REF.[134], CC BY 4.0.

TI interpretation challenged. The TI understanding of the (100) surface-state ARPES data has been strongly challenged[134] (FIG. 4). We begin with the α feature located at $\overline{X}$. The basic idea is shown in the schematic of FIG. 4b, which depicts different electronic structures for the bulk (solid line) and the surface (dashed line). The bulk structure corresponds to the hybridization-gap scenario from band theory, with E_F in the gap, and the surface structure is essentially a replica of the bulk structure, but surface shifted to deeper binding energy. If the shift is large enough relative to the magnitude of the gap, the effect is that E_F lies out of the surface gap, which creates a surface FS that is assigned to the α feature located at $\overline{X}$. So, the surface nature of the $\overline{X}$ ARPES FS is not challenged, but its origin as a TI surface state filling the bulk band gap

is discounted. Rather, it is understood as a topologically trivial surface-shifted conduction band extending all the way to the band minimum at $\overline{X}$.

Supporting this interpretation, there are two main ARPES findings from studies of cleaved (100) surfaces of float-zone samples, argued to result often in surfaces terminated exclusively either by Sm or B. First, there are spectra[134] that have been interpreted as showing that the surface *f*-states are shifted by about 10 meV to deeper binding energy relative to that of the bulk, as in FIG. 4b. Hybridization with this surface-shifted *f*-state is then proposed as the mechanism for the shifting of the surface conduction band of FIG. 4b. Second, there are variable photon-energy measurements for the bulk 5*d* band at an energy 65 meV below E_F, shown in FIG. 4a for a B-terminated surface. One can see both vertical streaks and a more complex variation, implying, respectively, both a surface k_z-independent and a bulk k_z-dependent character, as in FIG. 4b, even though the actual splitting of the surface and bulk conduction bands is not resolved. In the usual understanding of surface states, such a near-degeneracy with bulk states would leave such a surface state undefined due to decay into the bulk states. The counterargument made to this criticism is that the 4*f* states are so localized that the bulk and surface states are sufficiently spatially isolated from one another that this decay does not occur. In any case, there is some independent supporting evidence (J. D. Denlinger, personal communication, 2019) for the k_z-independent character and it does merit an explanation.

The scenario of FIG. 4b, presented in the preceding two paragraphs, must overcome two major barriers. First, as pointed out in the discussion of FIG. 3a, the bulk gap magnitude directly inferred by most researchers from photoemission data is 20 meV, in which case the *f*-state shift of 10 meV is too small for E_F to lie out of the surface gap. This difficulty motivated a very involved and, in our opinion, speculative argument[134] that the bulk gap magnitude is actually that of the much smaller resistivity activation energy, 4 meV. The putative small bulk gap was then further put forth as a rationale, alternative to that of the TI interpretation, for why the FS at $\overline{X}$ is so robust. In this rationale, all that would be required is any surface effect that shifts the *f*-state by more than the putative small bulk gap. However, if one adopts the epistemic principle of Occam's razor, the direct simplicity of the large-gap inference from numerous data like that of FIG. 3a tends to outweigh the speculative complexity of the small-gap argument. Second, the (100) SARPES results[124] of FIG. 3c,d are in direct contradiction with the scenario of FIG. 4b. This difficulty motivated a claim[134] that the (100) SARPES data should be entirely discounted. The reason[134] given for such extreme scepticism is that the SARPES group also reported[145] the observation of spin-polarized surface states for YbB_6, with the conclusion that it is a TI material, whereas it was subsequently shown[146] that YbB_6 is actually a non-TI insulator. However, this scepticism now seems too extreme. We note that the YbB_6 data do not appear to have been taken with the several extra precautions to show a surface-state origin, such as photon-polarization tests, described above for the SmB_6 (100) SARPES experiment. Further, the subsequent (111) SARPES findings[136] of FIG. 3f, obtained by an independent group, lend general credence to the (100) SARPES findings of FIG. 3c,d.

Certain aspects of the small (100) feature at $\overline{\Gamma}$ (FIG. 3a,b, as discussed above) also challenge the TI interpretation. First, it is not at all robust, as was shown and discussed in detail for Fig. 6 of REF.[117]. Second, as illustrated schematically in FIG. 4f, for a B-terminated surface of a float-grown sample, ARPES spectra in FIG. 4c,d for two ***k***-paths each show two parabolas that are oppositely offset in ***k*** from $\overline{\Gamma}$, which is characteristic of a spin–orbit split Rashba surface state. The measured FS map of FIG. 4e shows the implied double-ring $\overline{\Gamma}$ FS. REF.[134] assembles a number of other supporting arguments for the Rashba interpretation, including the fact that, for a Sm-terminated surface, the Rashba splitting is too small to observe, ascribed to the surface potential gradient being different for the two terminations. Thus far, no other ARPES group has replicated the Rashba surface-state observation. If this Rashba-split surface state was indeed the only $\overline{\Gamma}$ feature, then the TI interpretation would be rendered impossible because there would be an even number of surface-state FS pieces. However, the TI theory does not forbid the existence of other $\overline{\Gamma}$ surface states, such as the Rashba state, or the other non-robust small (100) features at $\overline{\Gamma}$ (FIG. 3a,b). For the TI interpretation, it is only essential that the (100) surface manifests a non-degenerate spin-polarized feature at Γ and, in fact, the data of FIG. 4c,e also show a very promising candidate, as we now discuss.

Reassignment of the α′ feature at $\overline{\Gamma}$. The data in FIG. 4c,e strongly motivate the hypothesis[136] that the Umklapp assignment of the large α′ feature at $\overline{\Gamma}$ is not correct, meaning that it does not come from the zone folding of $\overline{X}$ to $\overline{\Gamma}$. Rather, it is the predicted TI surface state at $\overline{\Gamma}$. The strong evidence supporting this hypothesis is almost overwhelming and very simply stated. First, the ARPES spectra of FIG. 4c also show the α′ feature very strongly, even though the surface being measured is B terminated, whereas the 2×1 reconstruction required for the Umklapp interpretation is found only for the Sm termination[55]. Second, one can note in the FS map of FIG. 4e that this feature appears to be better described as a circle than as either the oval that should occur for a single 1×2 domain or the more square shape that would result from a mix of 1×2 and 2×1 domains. The circular shape has been verified by analysis of both published and new, unpublished float-zone sample data (J. D. Denlinger, personal communication, 2019). Third, the magnitudes of the Fermi velocities of the α feature at $\overline{X}$ and the α′ feature at $\overline{\Gamma}$ are different, whereas they should always be identical for the Umklapp assignment. This can be quantified (J. D. Denlinger, personal communication, 2019) for the data of FIG. 4c and is obvious by eye in other data sets from this group (for example, FIGS 1d,2c of REF.[134] and Fig. 1 of REF.[61]). Fourth, its spin-momentum locking (FIG. 3c,d) shows that it is non-degenerate and, hence, enables the TI requirement for an odd number of TI states per unit cell of the surface BZ. Finally, and in sharp contrast to the other $\overline{\Gamma}$ surface states, the α′ feature is very robust.

To close this section, we compare the topological theory of FIG. 1 with the SARPES results in FIG. 3d,f, taking the (100) SARPES data at face value and taking the (100) α′ feature at $\overline{\Gamma}$ to be, indeed, an independent state. First, we see that all the features that are universal and dictated by topology are observed, that is, the (100) and (111) surfaces have surface states with spin-momentum locking at the expected locations, and, at high-symmetry planes, the spins are either parallel or anti-parallel to the arrows in FIG. 1. Second, assuming that the definitions of spin direction in the (100) and (111) experiments are consistent, we see that the winding senses for the two surfaces are opposite, so that the spins are parallel and anti-parallel to the FIG. 1 arrows, respectively. This conclusion, newly drawn here, has interesting implications for detailed microscopic theory. The $^6H_{5/2}$ multiplet, which gives rise to the six quasiparticle states involved in hybridization to form the gap (discussed above in connection with FIG. 3a), is actually crystal field split into a doublet and a quartet. One modelling simplification has been to include only one or the other of the two manifolds. The detailed microscopic theory of REF.[36] shows that the observed opposite winding senses of the two surfaces cannot be accommodated in such simplified models. A microscopic TI surface-state theory consistent with the new observation does not now exist but will require at least the inclusion of states from both manifolds.

Quantum oscillations

Quantum oscillations are another surprising phenomenon observed in the Kondo insulator SmB_6. Despite the more than seven orders of magnitude increases of the bulk resistivity with decreasing temperature, a quantum-oscillation pattern is observed in magnetic torque as a result of Landau-level quantizations[10] (FIG. 5).

Quantum oscillations usually arise from Landau-level quantization of an FS in a magnetic field. The quantization leads to oscillatory thermodynamic and transport properties, and yields rich information on the electronic structure, such as the FS orbit size, the effective mass and

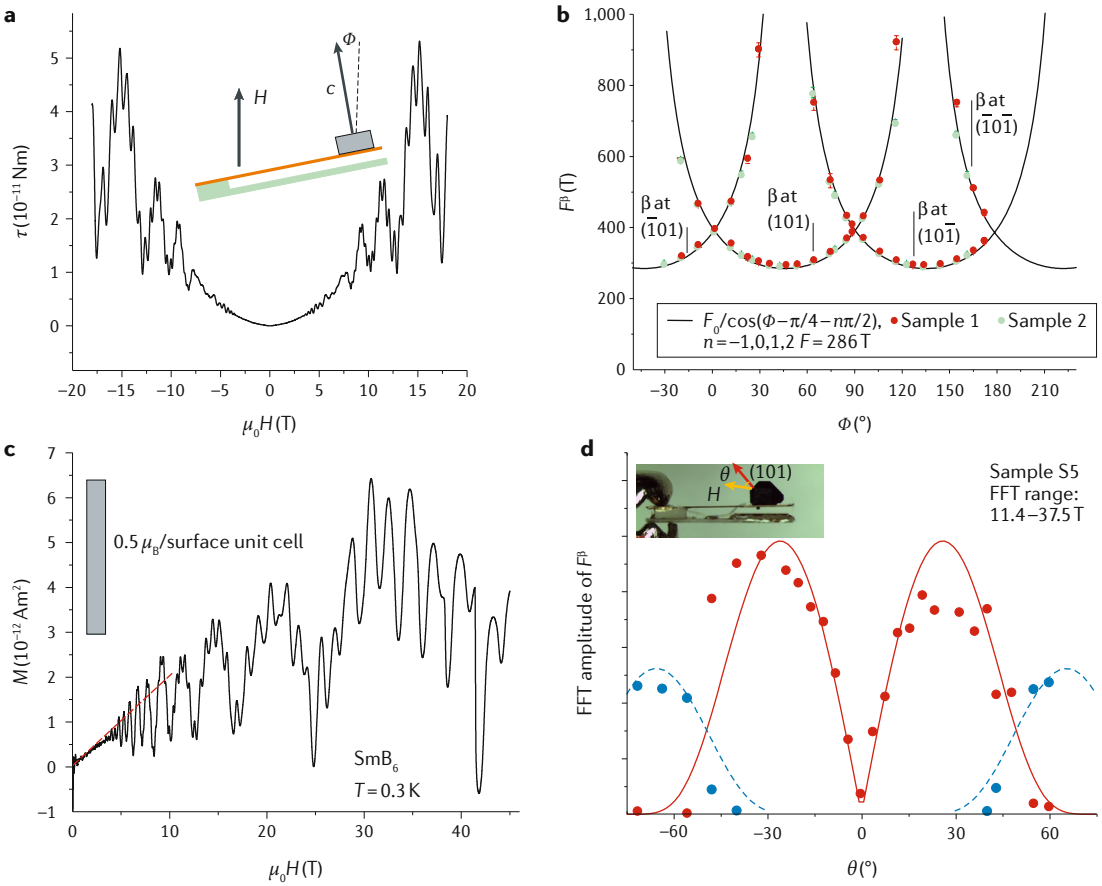

Fig. 5 | **Quantum oscillations in magnetization of SmB_6 indicating a 2D Fermi surface. a** | The magnetic torque of SmB_6 measured capacitively on the soft cantilever (pictured in inset) at 0.3 K. The magnetic torque starts to show an oscillatory pattern above 5 T. **b** | The dominating oscillation frequency follows the inverse sinusoidal dependence, indicating a 2D Fermi surface such as a cylindrical Fermi pocket with the long axis along the crystalline [110] directions. **c** | Magnetization, *M*, inferred by the magnetic torque versus magnetic field, *H*, shows a dominating oscillation pattern with an oscillation frequency on the order of 300–600 T. The dashed line shows that the effective volume magnetic susceptibility at low fields is 2.5×10^{-10} in the SI unit. **d** | In the irregularly shaped SmB_6 crystals, the oscillation amplitude of this dominating frequency breaks the fourfold rotational symmetry determined by the cubic bulk structure. The vertical axis is the oscillation amplitude determined by the fast Fourier transform (FFT). The symmetry breaking suggests that the surface roughness plays an essential role in determining the quantum oscillations. All the samples used in this panel were grown in flux. Panels **a**–**c** adapted with permission from REF.[10], AAAS. Panel **d** adapted from REF.[147], CC BY 4.0.

the scattering time. In particular, Landau-level quantizations lead to a magnetic susceptibility that oscillates periodically in the inverse of the magnetic field, B. The magnetic torque of a flux-grown SmB_6 single crystal is shown in FIG. 5a. The magnetic torque is measured capacitively on a soft cantilever. Above 5 T, the magnetic torque shows oscillations that are periodic in $1/B$. The angular dependence of the oscillatory frequency, for which the data are consistent with the 2D model, is shown in FIG. 5b. Pushing the magnetic-torque measurement up to 45-T magnetic fields resolves both slow and fast oscillations, which indicate a number of different oscillatory frequencies due to multiple FS orbits.

This observation leaves a mystery as to the origin of the oscillations. Landau-level quantizations happen in the FS of electrons, but it is unclear how an insulator can establish quantum oscillations. One possible explanation is the metallic surface state. By definition, the surface state is 2D and, thus, consistent with the observed angular dependence of oscillation frequencies.

The observation of quantum oscillations in magnetic torque was soon reproduced for floating-zone-grown single crystals, but a very different conclusion was drawn, that the oscillations actually arise from the bulk[16,48], presumably from an exotic spin-only neutral FS, because it is agreed that the material is a bulk insulator. There are two striking features. First, there are oscillation frequencies as large as 10,000 T, which is comparable to those of noble metals like copper or gold (FIG. 6a). Second, for the most dominating oscillation pattern, the oscillation amplitude at low temperatures deviates from the conventional Lifshitz–Kosevich model for Fermi-liquid theory. Instead, the amplitude increases dramatically at low temperatures (FIG. 6b).

Other than these two remarkable differences, the angular dependence of the observed oscillation frequencies in the new study (in the floating-zone-grown samples) is consistent with the early observations in flux-grown samples (FIG. 6c). The 3D FS model used in REFS[16,48] is extremely elongated ellipsoids, in contrast to the 2D cylindrical FS model used in early studies in REFS[10,147]. The sketch in FIG. 6d shows the overlap of these models for a large range of magnetic-field directions.

One argument for a bulk origin of these oscillations involves the oscillation amplitude, which is generally observed to be on the order of 10% of the background torque. The quadratic-field dependence of the background indicates a bulk origin and it is asserted that a surface layer could not produce oscillations with the observed magnitude comparable to that of the bulk background. This apparently straightforward argument is complicated by the fact that the torque signal requires an anisotropic magnetization, which is automatically very large for the surface, but for the bulk of simple-cubic-structured SmB_6, the leading order contribution is strictly zero due to the symmetry (P. Coleman, personal communication, 2019). This symmetry reduction of the bulk contribution can be seen in FIG. 5c, where the effective torque magnetization, $M_{eff} = \tau/B$, where τ is the torque, has a linear relationship with B, at $B < 10$ T. The effective magnetic susceptibility is only 2.5×10^{-10} (in the SI unit), compared with the bulk volume susceptibility[67] of 8.8×10^{-4}. This indicates that the calibrated anisotropic magnetization producing the background torque is reduced from the bulk magnetization by more than six orders of magnitude, so that the oscillation amplitude is then more than seven orders of magnitude smaller than the scalar product of the bulk magnetization and magnetic-field strength. This argument is consistent with the volume ratio of the surface layer and the entire crystal. A further discussion of intriguing open questions concerning the background, both its very small amplitude and its angle dependence, can be found in the Supplementary information.

To nail down the origin of the magnetization oscillations, surface or bulk, more experiments are needed, in particular, control experiments with different bulk volume, surface area and surface roughness. In one such control experiment, the oscillation amplitude of a flux-grown SmB_6 crystal with a somewhat irregular shape was measured[147]. For the same dominating oscillation frequency (FIG. 5c), the oscillation amplitude is tracked in various magnetic-field tilt angles. With the magnetic field rotated in the (010) plane, the quantum-oscillation frequency of this oscillation branch shows a fourfold rotational symmetry. However, in the angular dependence of the amplitude of the same branch, this fourfold symmetry is broken and, instead, a twofold symmetry appears[147]. The pattern is consistent with the prediction of a 2D Lifshitz–Kosevich model, with the variation of electric mobility of the surfaces. In other words, if the oscillation is actually a bulk phenomenon, it must, nonetheless, be able to manifest some properties characteristic of the surface, which would be a very complicated and unusual bulk scenario.

The bulk-oscillation picture may be supported in an indirect way by other evidence of bulk in-gap states. Heat-capacity measurements show a significant zero-magnetic-field, temperature-linear component at low temperatures, which is usually apparent in bulk metals[148]. A similar temperature-linear component is observed in some measurements of low-temperature thermal conductivity at finite magnetic fields[48], although other measurements gave negative reports[149,150]. Furthermore, the nuclear magnetic resonance spin relaxation time and the THz conductance shows indications of bulk in-gap states[49,151]. Also, Raman spectroscopy on floating-zone and flux-grown single crystals reveals a growth of gap-filling states as the Sm vacancy content of measured samples increases[152]. The measurements were performed on cleaved surfaces exposed to air.

Besides these electronic in-gap states, a bulk in-gap magnetic excitation near 14 meV is also observed in inelastic neutron scattering[51], as shown in FIG. 7a. An auxiliary-boson treatment of the lattice Anderson Hamiltonian with the minimal band model in FIG. 7b was found to give a good description of the mode dispersion, as shown by the dashed white lines in FIG. 7a. The model of FIG. 7b is also consistent with the general TI requirements. As mentioned earlier, an anomalous and puzzling finding is that the mode's energy-integrated momentum, $\mathbf{Q}$-dependence shown in FIG. 7c, is well described by the 5d form factor of the model, as shown in FIG. 7d, whereas one might have expected a 4f form

Lifshitz–Kosevich model
Also known as the Lifshitz–Kosevich formula, a theoretical formula describing the magnetic-field dependence of oscillatory physical properties as a result of the Landau-level quantizations in metals. A consequence of Landau's Fermi-liquid theory, the Lifshitz–Kosevich model explains particularly well the temperature dependence of the oscillatory magnitude of quantum oscillations.

Auxiliary-boson treatment
Also known as the auxiliary-boson method. Implies the use of any of several theoretical techniques for the study of strongly correlated quantum systems, where quantum dynamics and the effects of strong interactions among quantum particles are characterized through introducing additional (auxiliary) degrees of freedom.

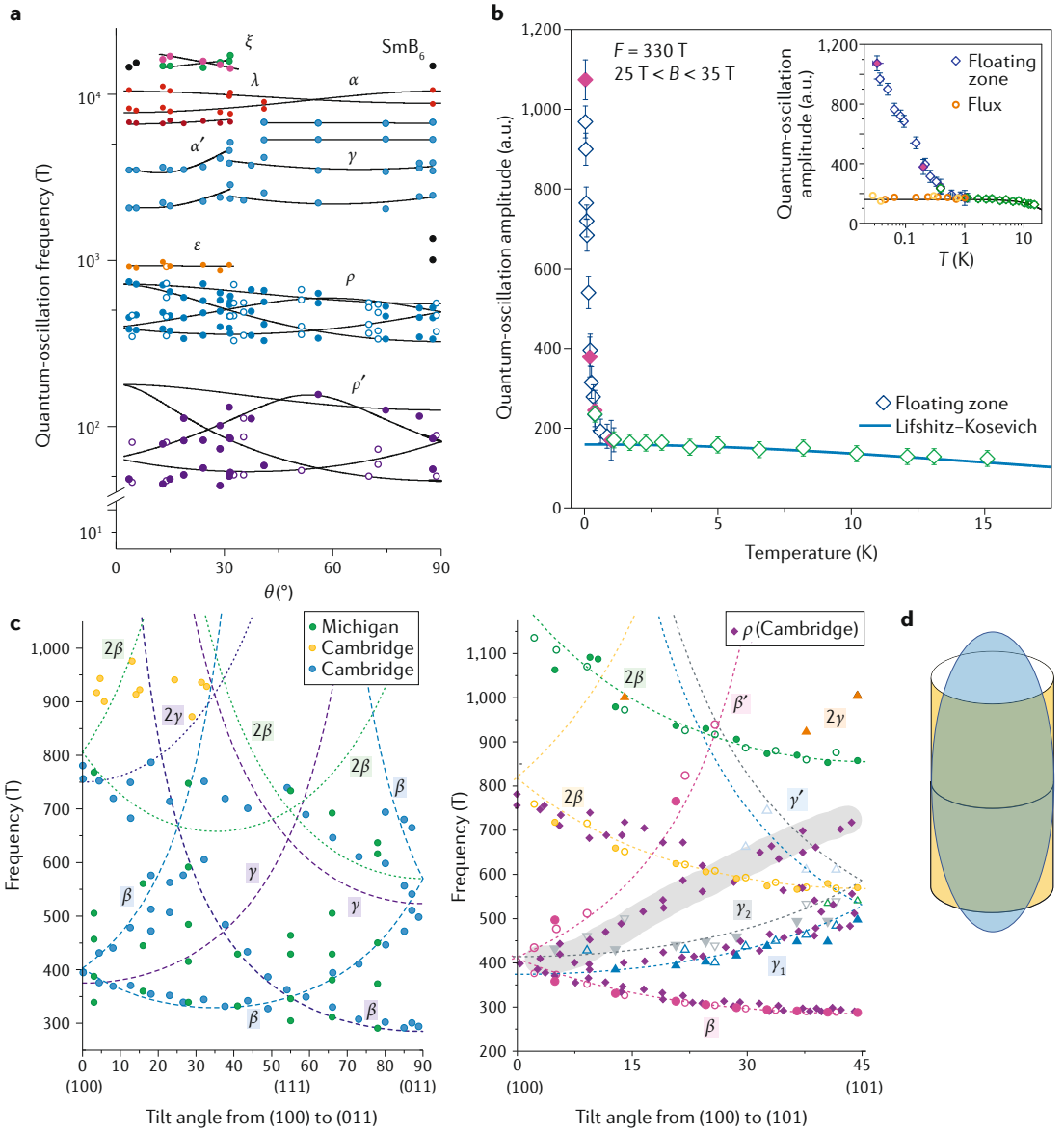

Fig. 6 | **Bulk quantum-oscillation pattern in SmB_6 crystals. a** | The angular dependences of oscillation frequencies suggest large bulk Fermi surfaces in the floating-zone-grown SmB_6 crystals. These pockets have oscillation frequencies in the range 1,000–20,000 T, with an orbit size similar to the bulk Brillouin zone. **b** | The dominating oscillation frequency of the floating-zone-grown crystal shows a temperature dependence deviating dramatically from the conventional Lifshitz–Kosevich dependence for a Fermi liquid, in contrast to the flux-grown crystals. This contrast is the most striking evidence for the unconventional Fermi surface in SmB_6. **c** | Comparison of the angular dependence of the oscillation frequencies of SmB_6 crystals measured by Li et al.[10] and Xiang et al. REF.[147] (labelled as Michigan) and by Tan et al.[16] and Hartstein et al.[48] (labelled as Cambridge) with magnetic field rotating from the crystalline [100] axis to the [111] axis and the [011] axis, and the same comparison with magnetic field rotating from the crystalline [100] axis to the [101] axis. The comparison shows that, for the dominating feature between 300 T and 1,000 T, the angular dependences in these crystals are consistent within the scattering of these data. The most notable difference is marked within the shaded area. **d** | A sketch compares the 2D cylindrical Fermi surface model and a 3D extremely elongated ellipsoidal Fermi surface model. Panel **a** adapted with permission from REF.[16], AAAS. Panel **b** adapted from REF.[48], Springer Nature Limited. Panel **c** adapted from REF.[147], CC BY 4.0.

factor. Also highly relevant here, such measurements are a direct probe for the single-particle spin excitations that would be expected to underlie the conjectured spin-only neutral bulk FS. But in these most recent and sensitive measurements, the observed spectra below 50 meV are said to be dominated by the collective mode. No other excitations were reported.

Finally, returning to the main topic of this section, the most puzzling mystery is the lack of quantum oscillations in the electrical resistance. Traditionally, the resistance measurement is the only tool used to resolve quantum oscillations of the surface state. For the surface state of the topological Kondo insulator, nothing would block the surface metallic state from the observation of

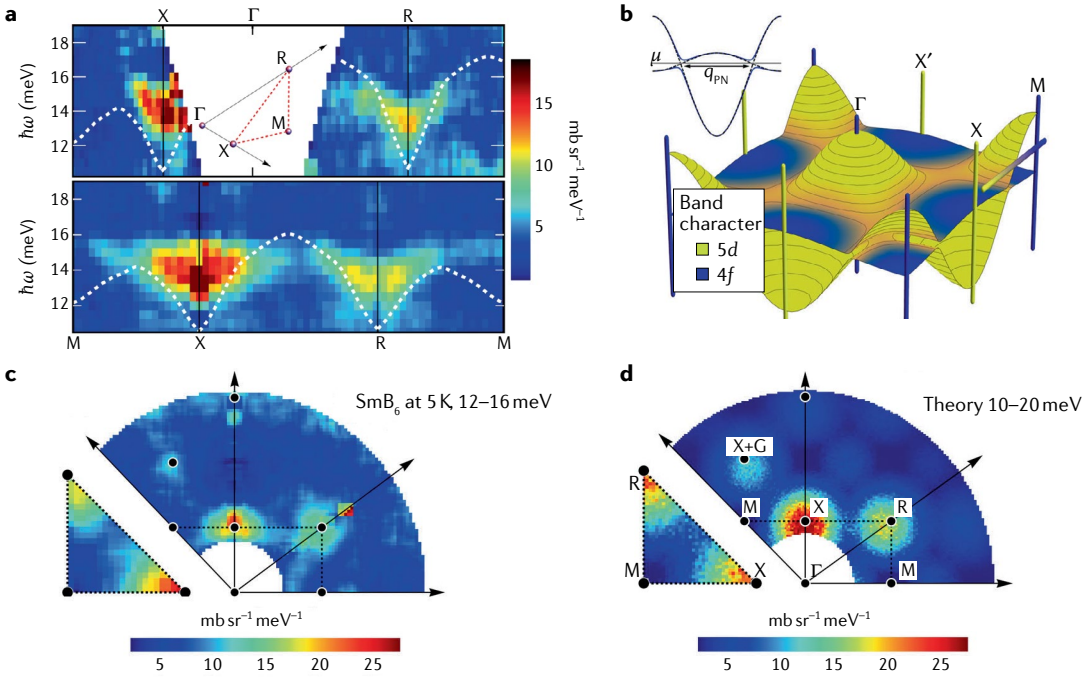

Fig. 7 | **Bulk magnetic excitations of SmB_6. a** | Inelastic neutron-scattering cross section for $^{154}Sm^{11}B_6$ at 5 K along high-symmetry directions (inset), from the Γ point (top) and around the Brillouin zone edges (bottom). The dashed line shows the dispersion of a boson-mediated exciton calculated for the band structure of panel **b**. **b** | Phenomenological minimal topological insulator band structure model within the (*hk*0) crystal plane to describe data in panel **a**. Translation from X to M shows the change in band character. The inset shows a schematic representation of pseudo-nesting vectors. **c** | Energy-integrated neutron-scattering intensity in high-symmetry plane at 5 K. **d** | A theoretical description of the data in panel **c**, provided by the momentum **Q**-dependence of $\chi_0(\mathbf{Q})|F(\mathbf{Q})|^2$, where $\chi_0(\mathbf{Q})$ is the Lindhardt susceptibility for the band structure in panel **b** and $F(\mathbf{Q})$ is the 5*d* electron form factor. Adapted with permission from REF.[51], APS.

Landau-level quantizations. Yet, despite intense efforts of the community, all the reported quantum-oscillation studies have failed to resolve an oscillatory resistivity. In particular, pushing the magnetoresistance to magnetic fields as high as 85 T does not resolve quantum oscillations. Testing in other topological-Kondo-insulator candidates eventually shows quantum oscillations in both magnetization and electrical resistance in the insulating state at intense magnetic fields[153,154]. However, the mystery remains as to the origin of magnetic quantum oscillations in SmB_6.

Discussion

We conclude with final thoughts presented as three elaborated questions.

What makes SmB_6 worth studying? The nature of its correlated electron ground state is a paradigmatic problem of strongly correlated condensed-matter physics. Even in the earliest studies, there was vigorous debate. Examples include arguments that a gap is impossible[155] or that the Luttinger theorem, introduced by Richard Martin to discuss single particle gaps and FS in the mixed-valent and Kondo-lattice problems[76,141,156], is not applicable[157]. An insulator model competing with the single-particle Fermi-liquid gap model was an exciton picture in which the 5*d* electrons freed in the valence mixing process remain bound to Sm^{3+} $4f^5$ sites[71,158]. This model was later used to explain early neutron-scattering results[159]. A later augmentation of the theory[160] introduced a conducting exciton–polaron band inside a single-particle gap, argued to explain the low-temperature resistivity plateau by evading single-particle resistivity-limit theorems.

In our opinion, the basic TI predictions (FIG. 1c–e) are strongly supported by the spin-dependent transport measurements[14,91–94] and the SARPES results (FIG. 3d,f), some remaining ARPES issues notwithstanding. This finding then weighs strongly in favour of the single-particle Fermi-liquid gap and also greatly constrains theories for non-trivial bulk quasiparticle excitations beyond the theory of Landau. This leaves two options. Either a single-phase theory of such a state must also produce surface states with the same topological properties as observed, which has not been shown for any such theory to date. Alternatively, the clear possibility of two separate phases that could coexist in samples must be established, both in experiments and in theory. The strongest theoretical case for such phase compatibility would be a demonstration that both phases can be derived from starting points that share the underlying, characteristic, essential elements of the SmB_6 electronic structure, differing only by the variation of one or more control parameters that could be physically realized, for example, by hydrostatic pressure, uniaxial stress, magnetic field or some consequence of the method of sample preparation, such as stoichiometry variation. There is also no theory for what is perhaps the most remarkable bulk property, clearly established experimentally (FIG. 2e), the extreme robustness of the bulk gap against conduction due to impurities. A hint of

understanding for this may lie in the theory in REF.[161] of topological non-magnetic impurity states in topological Kondo insulators, where metallic states form on shells neighbouring the impurity and act to surround the defect, analogous to the metallic surface states that surround the TI bulk.

A corollary to the first question is, how correlated are the surface states of SmB_6? The Kondo insulator is known to host strong electronic interactions in its bulk. As a result, the effective mass of the surface states has generally been expected to be large. Experimental evidence shows a rather complicated picture. The measured effective mass m varies in different experiments: $m \sim 0.2–1\ m_e$ (electron mass) in quantum-oscillation experiments[48], $m \sim 3–15\ m_e$ in photoemission[12,39,117,119,120,126,134] and $m \sim 100–1{,}000\ m_e$ in scanning tunnelling spectroscopy[60]. Further, even though the mapping based on the quasiparticle interference resolves a heavy mass and a small Fermi velocity[60], the planar junction tunnelling[162] determined a set of faster Fermi velocities that is consistent with the early quantum-oscillation studies (Table S1b in the Supplementary Information)[162]. The variation suggests that different experimental techniques probe different electronic structures.

How can we move forwards experimentally? In the absence of a totally new experimental approach, which we do not try to offer here, it would be a major step forwards to understand exactly how the sample growth and/or preparation conditions affect the physical observations. As evident from our review discussions, and summarized in detail in Table S1b of the Supplementary Information, much of the critical experimental evidence depends on the growth technique for the SmB_6 crystals. For example, the most striking feature of the bulk 3D FS was observed only in quantum oscillations in floating-zone-grown crystals, and, arguably, such crystals have yielded the best-resolved ARPES data. Questions arise as to what happens in these growth and preparation processes. Aluminium flux growth may leave traces of crystalline aluminium inside SmB_6 crystals, which has been argued to be the origin of the quantum oscillations observed in flux-grown SmB_6 crystals[163]. By contrast, the extremely high growth temperature used in the floating-zone-grown method may likely leave lots of vacancies. As a result, the valence may go up to 3+ in these defects (Z. Fisk, Personal communication, 2019), which could lead to local magnetic moments and even a smaller lattice constant.One possible solution to this sample issue is to find a new method for clean, single-crystal growth of SmB_6. A flux method without Al flux would be ideal, so that the growth temperature is still low enough not to produce many vacancies. However, a different flux material will have a lattice constant quite different from SmB_6, which leads to less chance of embedding crystalline flux inside crystals. Alternatively, extending these experiments to samples screened for Al inclusions can be particularly valuable, and the community needs to develop a reliable experimental probe to detect Al inclusions without mechanically polishing, which risks damaging the surface and affecting the surface-state Sm valences of the samples.

But, in general, we encourage experimentalists to work systematically with samples grown by different methods and try to identify if there are materials issues associated with the observed differences in all experimental findings. In particular, so doing could be one way to search for clear evidence of the two separate ground-states phases mentioned in the discussion under the first question above, perhaps coupled with studies to see if some combination of external perturbations like hydrostatic pressure, uniaxial stress or magnetic field could induce the same property differences as found for different sample-growth methods.

Where are all the other f-electron materials? No fewer than 16 rare-earth and actinide compounds that are also small-gap semiconductors are listed in Table I in REF.[164]. But in the 8 years since the first evidence for TI surface states in SmB_6 appeared, it remains the prime object of study. The only other mixed-valent *f*-electron material that has been studied for TI properties is YbB_{12} by ARPES[165], and, in this case, the high magnetic-field oscillations happen in a magnetic field within 10 T of the gap-closing field[153]. It seems possible that, if a number of other examples could be found and studied at the same depth as SmB_6, a synergism would emerge[166]. There has been a recent development of interest in possible topological properties of some *d*-electron insulators, such as FeSi (REF.[167]) and $FeSb_2$ (REF.[168]). The gaps of these materials have a correlated character and experimental evidence of metallic surface states is found. Even though they are sometimes characterized as Kondo insulators[164,169], their photoemission spectra do not manifest the evidences of the very strong correlations found in the *f*-electron materials, such as atomic-like multiplets, or even clear Hubbard band satellites. So these materials are likely to yield different insights into the general problem of correlated insulators, relative to those from materials like SmB_6.

Published online: 05 August 2020

1. Hasan, M. Z. et al. Colloquium: topological insulators. *Rev. Mod. Phys.* **82**, 3045 (2010).
2. Qi, X.-L. et al. Topological insulators and superconductors. *Rev. Mod. Phys.* **83**, 1057 (2011).
3. Varma, C. Mixed-valence compounds. *Rev. Mod. Phys.* **48**, 219 (1976).
4. Menth, A. et al. Magnetic and semiconducting properties of SmB_6. *Phys. Rev. Lett.* **22**, 295 (1969).
5. Dzero, M. et al. Topological Kondo insulators. *Phys. Rev. Lett.* **104**, 106408 (2010).
This letter proposed the concept of topological Kondo insulators and theoretically predicted that such a topological state shall emerge in heavy fermion insulators such as SmB_6.
6. Dzero, M. et al. Topological Kondo insulators. *Annu. Rev. Condens. Matter Phys.* **7**, 249–280 (2016).
7. Wolgast, S. et al. Low-temperature surface conduction in the Kondo insulator SmB_6. *Phys. Rev. B* **88**, 180405 (2013).
This paper presents one of the first indications of the surface states in SmB_6.
8. Zhang, X. et al. Hybridization, inter-ion correlation, and surface states in the Kondo insulator SmB_6. *Phys. Rev. X* **3**, 011011 (2013).
This paper shows another of the first indications of the surface states in SmB_6.
9. Kim, D. J. et al. Surface Hall effect and nonlocal transport in SmB_6: evidence for surface conduction. *Sci. Rep.* **3**, 3150 (2013).
This paper is also one of the first indications of the surface states in SmB_6.
10. Li, G. et al. Two-dimensional Fermi surfaces in Kondo insulator SmB_6. *Science* **346**, 1208–1212 (2014).
This study is the first report of the quantum oscillations in magnetization in Kondo insulators.
11. Rößler, S. et al. Hybridization gap and Fano resonance in SmB_6. *Proc. Natl Acad. Sci. USA* **111**, 4798–4802 (2014).
12. Xu, N. et al. Surface and bulk electronic structure of the strongly correlated system SmB_6 and implications

for a topological Kondo insulator. *Phys. Rev. B* **88**, 121102 (2013).
First of the early reports of surface states observed by ARPES in SmB_6.
13. Neupane, M. et al. Non-Kondo-like electronic structure in the correlated rare-earth hexaboride YbB_6. *Phys. Rev. Lett.* **114**, 016403 (2015).
14. Song, Q. et al. Spin injection and inverse Edelstein effect in the surface states of topological Kondo insulator SmB_6. *Nat. Commun.* **7**, 13485 (2016).
15. Lee, S. et al. Observation of the superconducting proximity effect in the surface state of SmB_6 thin films. *Phys. Rev. X* **6**, 031031 (2016).
16. Tan, B. S. et al. Unconventional Fermi surface in an insulating state. *Science* **349**, 287–290 (2015).
17. Knolle, J. et al. Excitons in topological Kondo insulators: theory of thermodynamic and transport anomalies in SmB_6. *Phys. Rev. Lett.* **118**, 096604 (2017).
18. Erten, O. et al. Skyrme insulators: insulators at the brink of superconductivity. *Phys. Rev. Lett.* **119**, 057603 (2017).
19. Chowdhury, D. et al. Mixed-valence insulators with neutral Fermi surfaces. *Nat. Commun.* **9**, 1766 (2018).
20. Sodemann, I. et al. Quantum oscillations in insulators with neutral Fermi surfaces. *Phys. Rev. B* **97**, 045152 (2018).
21. Lai, H.-H. et al. Weyl–Kondo semimetal in heavy-fermion systems. *Proc. Natl Acad. Sci. USA* **115**, 93–97 (2018).
22. Dresselhaus, M. S. et al. *Group Theory: Application to the Physics of Condensed Matter* (Springer, 2008).
23. Bradlyn, B. et al. Topological quantum chemistry. *Nature* **547**, 298–305 (2017).
24. Po, H. C. et al. Symmetry-based indicators of band topology in the 230 space groups. *Nat. Commun.* **8**, 50 (2017).
25. Song, Z. et al. Quantitative mappings between symmetry and topology in solids. *Nat. Commun.* **9**, 3530 (2018).
26. Song, Z. et al. Diagnosis for nonmagnetic topological semimetals in the absence of spin-orbital coupling. *Phys. Rev. X* **8**, 031069 (2018).
27. Kruthoff, J. et al. Topological classification of crystalline insulators through band structure combinatorics. *Phys. Rev. X* **7**, 041069 (2017).
28. Zhang, T. et al. Catalogue of topological electronic materials. *Nature* **566**, 475–479 (2019).
29. Vergniory, M. G. et al. A complete catalogue of high-quality topological materials. *Nature* **566**, 480–485 (2019).
30. Tang, F. et al. Comprehensive search for topological materials using symmetry indicators. *Nature* **566**, 486–489 (2019).
31. Fu, L. et al. Topological insulators with inversion symmetry. *Phys. Rev. B* **76**, 045302 (2007).
32. Fang, C. et al. Bulk topological invariants in noninteracting point group symmetric insulators. *Phys. Rev. B* **86**, 115112 (2012).
33. Ye, M. et al. Topological crystalline Kondo insulators and universal topological surface states of SmB_6. Preprint at *arXiv* https://arxiv.org/abs/1307.7191 (2013).
34. Baruselli, P. P. et al. Distinct topological crystalline phases in models for the strongly correlated topological insulator SmB_6. *Phys. Rev. Lett.* **115**, 156404 (2015).
35. Legner, M. et al. Surface-state spin textures and mirror Chern numbers in topological Kondo insulators. *Phys. Rev. Lett.* **115**, 156405 (2015).
36. Baruselli, P. P. et al. Spin textures on general surfaces of the correlated topological insulator SmB_6. *Phys. Rev. B* **93**, 195117 (2016).
37. Lu, F. et al. Correlated topological insulators with mixed valence. *Phys. Rev. Lett.* **110**, 096401 (2013).
38. Thunström, P. et al. Multiplet effects in the electronic structure of intermediate-valence compounds. *Phys. Rev. B* **79**, 165104 (2009).
39. Denlinger, J. D. et al. Temperature dependence of linked gap and surface state evolution in the mixed valent topological insulator SmB_6. Preprint at *arXiv* https://arxiv.org/abs/1312.6637 (2013).
40. Kim, J. et al. Termination-dependent surface in-gap states in a potential mixed-valent topological insulator: SmB_6. *Phys. Rev. B* **90**, 075131 (2014).
41. Shick, A. B. et al. Racah materials: role of atomic multiplets in intermediate valence systems. *Sci. Rep.* **5**, 15429 (2015).
42. Peters, R. et al. Coexistence of light and heavy surface states in a topological multiband Kondo insulator. *Phys. Rev. B* **93**, 235159 (2016).
43. Thunström, P. et al. Topology of SmB_6 determined by dynamical mean field theory. Preprint at *arXiv* https://arxiv.org/abs/1907.03899 (2019).
44. Werner, J. et al. Dynamically generated edge states in topological Kondo insulators. *Phys. Rev. B* **89**, 245119 (2014).
45. Knolle, J. et al. Quantum oscillations without a Fermi surface and the anomalous de Haas–van Alphen effect. *Phys. Rev. Lett.* **115**, 146401 (2015).
46. Shen, H. et al. Quantum oscillation from in-gap states and a non-Hermitian Landau level problem. *Phys. Rev. Lett.* **121**, 026403 (2018).
47. Harrison, N. Highly asymmetric nodal semimetal in bulk SmB_6. *Phys. Rev. Lett.* **121**, 026602 (2018).
48. Hartstein, M. et al. Fermi surface in the absence of a Fermi liquid in the Kondo insulator SmB_6. *Nat. Phys.* **14**, 166–172 (2017).
49. Laurita, N. J. et al. Anomalous three-dimensional bulk ac conduction within the Kondo gap of SmB_6 single crystals. *Phys. Rev. B* **94**, 165154 (2016).
50. Fuhrman, W. T. et al. Screened moments and extrinsic in-gap states in samarium hexaboride. *Nat. Commun.* **9**, 1539 (2018).
51. Fuhrman, W. T. et al. Interaction driven subgap spin exciton in the Kondo insulator SmB_6. *Phys. Rev. Lett.* **114**, 036401 (2015).
52. Canfield, P. C. et al. Growth of single crystals from metallic fluxes. *Philos. Mag. B* **65**, 1117–1123 (1992).
53. Balakrishnan, G. et al. Growth of large single crystals of rare earth hexaborides. *J. Cryst. Growth* **256**, 206–209 (2003).
54. Ruan, W. et al. Emergence of a coherent in-gap state in the SmB_6 Kondo insulator revealed by scanning tunneling spectroscopy. *Phys. Rev. Lett.* **112**, 136401 (2014).
55. Rößler, S. et al. Surface and electronic structure of SmB through scanning tunneling microscopy. *Philos. Mag.* **96**, 3262–3273 (2016).
56. Jiao, L. et al. Additional energy scale in SmB_6 at low-temperature. *Nat. Commun.* **7**, 13762 (2016).
57. Miyamachi, T. et al. Evidence for in-gap surface states on the single phase SmB_6(001) surface. *Sci. Rep.* **7**, 12837 (2017).
58. Sun, Z. et al. Observation of a well-defined hybridization gap and in-gap states on the SmB_6 (001) surface. *Phys. Rev. B* **97**, 235107 (2018).
59. Jiao, L. et al. Magnetic and defect probes of the SmB_6 surface state. *Sci. Adv.* **4**, eaau4886 (2018).
60. Pirie, H. et al. Imaging emergent heavy Dirac fermions of a topological Kondo insulator. *Nat. Phys.* **16**, 52–56 (2020).
61. Herrmann, H. et al. Contrast reversal in scanning tunneling microscopy and its implications for the topological classification of SmB_6. *Adv. Mater.* **32**, 1906725 (2020).
62. Heming, N. et al. Surface properties of SmB_6 from x-ray photoelectron spectroscopy. *Phys. Rev. B* **90**, 195128 (2014).
63. Lutz, P. et al. Valence characterisation of the subsurface region in SmB_6. *Philos. Mag.* **96**, 3307–3321 (2016).
64. He, H. et al. Irreversible proliferation of magnetic moments at cleaved surfaces of the topological Kondo insulator SmB_6. *Phys. Rev. B* **95**, 195126 (2017).
65. Zabolotnyy, V. B. et al. Chemical and valence reconstruction at the surface of SmB_6 revealed by means of resonant soft x-ray reflectometry. *Phys. Rev. B* **97**, 205416 (2018).
66. Paderno, Y. B. et al. Electrical properties of hexaborides of the alkaline- and rare-earth metals at low temperatures. *Sov. Powder Metall. Met. Ceram.* **8**, 921–923 (1969).
67. Cohen, R. L. et al. Electronic and magnetic structure of SmB_6. *Phys. Rev. Lett.* **24**, 383 (1970).
68. Allen, J. W. et al. Large low-temperature Hall effect and resistivity in mixed-valent SmB_6. *Phys. Rev. B* **20**, 4807 (1979).
First report of Hall-effect data proving that SmB_6 is an insulator.
69. Cooley, J. C. et al. SmB_6: Kondo insulator or exotic metal? *Phys. Rev. Lett.* **74**, 1629 (1995).
70. Coleman, P. et al. Theory for the anomalous Hall constant of mixed-valence systems. *Phys. Rev. Lett.* **55**, 414 (1985).
71. Nickerson, J. C. et al. Physical properties of SmB_6. *Phys. Rev. B* **3**, 2030 (1971).
72. von Molnar, S. et al. in *Valence Instabilities: Proceedings of the International Conference* (eds Wachter, P. et al.) 385 (North Holland, 1982).
73. Stankiewicz, J. et al. Physical properties of Sm_xB_6 single crystals. *Phys. Rev. B* **99**, 045138 (2019).
74. Rakoski, A. et al. Investigation of high-temperature bulk transport characteristics and skew scattering in samarium hexaboride. *J. Supercond. Nov. Magn.* **33**, 265–268 (2020).
75. Mott, N. F. Rare-earth compounds with mixed valencies. *Philos. Mag.* **30**, 403–416 (1974).
76. Martin, R. M. et al. Theory of mixed valence: Metals or small gap insulators (invited). *J. Appl. Phys.* **50**, 7561 (1979).
77. Riseborough, P. S. The electrical resistivity of mixed valence materials due to impurities. *Solid State Commun.* **38**, 79–82 (1981).
78. Travaglini, G. et al. Intermediate-valent SmB_6 and the hybridization model: An optical study. *Phys. Rev. B* **29**, 893 (1984).
79. Gorshunov, B. et al. Low-energy electrodynamics of SmB_6. *Phys. Rev. B* **59**, 1808 (1999).
80. Nozawa, S. et al. Ultrahigh-resolution and angle-resolved photoemission study of SmB_6. *J. Phys. Chem. Solids* **63**, 1223–1226 (2002).
81. Miyazaki, H. et al. Momentum-dependent hybridization gap and dispersive in-gap state of the Kondo semiconductor SmB_6. *Phys. Rev. B* **86**, 075105 (2012).
82. Flachbart, K. et al. Energy gap of intermediate-valent SmB_6 studied by point-contact spectroscopy. *Phys. Rev. B* **64**, 085104 (2001).
83. Chen, F. et al. Magnetoresistance evidence of a surface state and a field-dependent insulating state in the Kondo insulator SmB_6. *Phys. Rev. B* **91**, 205133 (2015).
84. Yue, Z. et al. Crossover of magnetoresistance from fourfold to twofold symmetry in SmB_6 single crystal, a topological Kondo insulator. *J. Phys. Soc. Jpn.* **84**, 044717 (2015).
85. Wolgast, S. et al. Magnetotransport measurements of the surface states of samarium hexaboride using Corbino structures. *Phys. Rev. B* **92**, 115110 (2015).
86. Wakeham, N. et al. Surface state reconstruction in ion-damaged SmB_6. *Phys. Rev. B* **91**, 085107 (2015).
87. Lu, H.-Z. et al. Weak localization of bulk channels in topological insulator thin films. *Phys. Rev. B* **84**, 125138 (2011).
88. Dzero, M. et al. Nonuniversal weak antilocalization effect in cubic topological Kondo insulators. *Phys. Rev. B* **92**, 165415 (2015).
89. Thomas, S. et al. Weak antilocalization and linear magnetoresistance in the surface state of SmB_6. *Phys. Rev. B* **94**, 205114 (2016).
90. Nakajima, Y. et al. One-dimensional edge state transport in a topological Kondo insulator. *Nat. Phys.* **12**, 213–217 (2016).
91. Kim, J. et al. Electrical detection of the surface spin polarization of the candidate topological Kondo insulator SmB_6. *Phys. Rev. B* **99**, 245148 (2019).
92. Geurs, J. et al. Anomalously large spin-current voltages on the surface of SmB_6. *Phys. Rev. B* **100**, 035435 (2019).
93. Liu, T. et al. Nontrivial nature and penetration depth of topological surface states in SmB_6 thin films. *Phys. Rev. Lett.* **120**, 207206 (2018).
94. Lee, S. et al. Perfect Andreev reflection due to the Klein paradox in a topological superconducting state. *Nature* **570**, 344–348 (2019).
95. Yong, J. et al. Robust topological surface state in Kondo insulator SmB_6 thin films. *Appl. Phys. Lett.* **105**, 222403 (2014).
96. Yong, J. et al. Magnetotransport in nanocrystalline SmB_6 thin films. *AIP Adv.* **5**, 077144 (2015).
97. Shishido, H. et al. Semi-epitaxial SmB_6 thin films prepared by the molecular beam epitaxy. *Phys. Procedia* **75**, 405–412 (2015).
98. Shaviv Petrushevsky, M. et al. Signature of surface state coupling in thin films of the topological Kondo insulator SmB_6 from anisotropic magnetoresistance. *Phys. Rev. B* **95**, 085112 (2017).
99. Batkova, M. et al. Electrical properties of SmB_6 thin films prepared by pulsed laser deposition from a stoichiometric SmB_6 target. *J. Alloy. Compd.* **744**, 821–827 (2018).
100. Wolgast, S. et al. Conduction through subsurface cracks in bulk topological insulators. Preprint at *arXiv* https://arxiv.org/abs/1506.08233 (2015).
101. Eo, Y. S. et al. Comprehensive surface magnetotransport study of SmB_6. *Phys. Rev. B* **101**, 155109 (2020).
102. Syers, P. et al. Tuning bulk and surface conduction in the proposed topological Kondo insulator SmB_6. *Phys. Rev. Lett.* **114**, 096601 (2015).
103. Wolgast, S. et al. Reduction of the low-temperature bulk gap in samarium hexaboride under high magnetic fields. *Phys. Rev. B* **95**, 245112 (2017).

104. Zhou, Y. et al. Quantum phase transition and destruction of Kondo effect in pressurized SmB_6. *Sci. Bull.* **62**, 1439–1444 (2017).
105. Cooley, J. C. et al. High field gap closure in the Kondo insulator SmB_6. *J. Supercond.* **12**, 171–173 (1999).
106. Kang, B. Y. et al. Magnetic and nonmagnetic doping dependence of the conducting surface states in SmB_6. *Phys. Rev. B* **94**, 165102 (2016).
107. Kim, D. J. et al. Topological surface state in the Kondo insulator samarium hexaboride. *Nat. Mater.* **13**, 466–470 (2014).
108. Eo, Y. S. et al. Inverted resistance measurements as a method for characterizing the bulk and surface conductivities of three-dimensional topological insulators. *Phys. Rev. Appl.* **9**, 044006 (2018).
109. Eo, Y. S. et al. Transport gap in SmB_6: protected against disorder. *Proc. Natl Acad. Sci. USA* **116**, 12638–12641 (2019).
This study reveals the robust bulk insulating gap in SmB_6.
110. Rakoski, A. et al. Understanding low-temperature bulk transport in samarium hexaboride without relying on in-gap bulk states. *Phys. Rev. B* **95**, 195133 (2017).
111. Bardeen, J. et al. Theory of superconductivity. *Phys. Rev.* **108**, 1175 (1957).
112. Skinner, B. Properties of the donor impurity band in mixed valence insulators. *Phys. Rev. Mater.* **3**, 104601 (2019).
113. Woolf, M. A. et al. Effect of magnetic impurities on the density of states of superconductors. *Phys. Rev.* **137**, A557 (1965).
114. Cardona, M. et al. (eds) *Photoemission in Solids I: General Principles* (Springer, 1978).
115. Bardyszewski, W. et al. A new approach to the theory of photoemission from solids. *Phys. Scr.* **32**, 439 (1985).
116. Himpsel, F. J. Angle-resolved measurements of the photoemission of electrons in the study of solids. *Adv. Phys.* **32**, 1–51 (1983).
117. Denlinger, J. D. et al. in *Proc. Int. Conf. Strongly Correlated Electron Systems (SCES2013)* Vol. 3 JPS Conference Proceedings 017038 (The Physical Society of Japan, 2014).
118. Smith, N. V. et al. Photoemission linewidths and quasiparticle lifetimes. *Phys. Rev. B* **47**, 15476 (1993).
119. Jiang, J. et al. Observation of possible topological in-gap surface states in the Kondo insulator SmB_6 by photoemission. *Nat. Commun.* **4**, 3010 (2013).
120. Neupane, M. et al. Surface electronic structure of the topological Kondo-insulator candidate correlated electron system SmB_6. *Nat. Commun.* **4**, 2991 (2013).
121. Zhu, Z. H. et al. Polarity-driven surface metallicity in SmB_6. *Phys. Rev. Lett.* **111**, 216402 (2013).
122. Frantzeskakis, E. et al. Kondo hybridization and the origin of metallic states at the (001) surface of SmB_6. *Phys. Rev. X* **3**, 041024 (2013).
123. Suga, S. et al. Spin-polarized angle-resolved photoelectron spectroscopy of the so-predicted Kondo topological insulator SmB_6. *J. Phys. Soc. Jpn.* **83**, 014705 (2014).
124. Xu, N. et al. Direct observation of the spin texture in SmB_6 as evidence of the topological Kondo insulator. *Nat. Commun.* **5**, 4566 (2014).
This paper is the first direct observation of spin-textured surface states in SmB_6.
125. Min, C.-H. et al. Importance of charge fluctuations for the topological phase in SmB_6. *Phys. Rev. Lett.* **112**, 226402 (2014).
126. Xu, N. et al. Exotic Kondo crossover in a wide temperature region in the topological Kondo insulator SmB_6 revealed by high-resolution ARPES. *Phys. Rev. B* **90**, 085148 (2014).
127. Ishida, Y. et al. Emergent photovoltage on SmB_6 surface upon bulk-gap evolution revealed by pump-and-probe photoemission spectroscopy. *Sci. Rep.* **5**, 8160 (2015).
128. Min, C.-H. et al. Two-component analysis of the *4f* multiplet of samarium hexaboride. *J. Electron Spectrosc. Relat. Phenom.* **199**, 46–50 (2015).
129. Ellguth, M. et al. Momentum microscopy of single crystals with detailed surface characterisation. *Philos. Mag.* **96**, 3284–3306 (2016).
130. Arab, A. et al. Effects of spin excitons on the surface states of SmB_6: a photoemission study. *Phys. Rev. B* **94**, 235125 (2016).
131. Ramankutty, S. V. et al. Comparative study of rare earth hexaborides using high resolution angle-resolved photoemission. *J. Electron Spectrosc. Relat. Phenom.* **208**, 43–50 (2016).
132. Utsumi, Y. et al. Bulk and surface electronic properties of SmB_6: A hard x-ray photoelectron spectroscopy study. *Phys. Rev. B* **96**, 155130 (2017).
133. Min, C.-H. et al. Matching DMFT calculations with photoemission spectra of heavy fermion insulators: universal properties of the near-gap spectra of SmB_6. *Sci. Rep.* **7**, 11980 (2017).
134. Hlawenka, P. et al. Samarium hexaboride is a trivial surface conductor. *Nat. Commun.* **9**, 517 (2018).
135. Ohtsubo, Y. et al. Surface electronic structure of SmB_6 (111). *Physica B Condens. Matter* **536**, 75–77 (2018).
136. Ohtsubo, Y. et al. Non-trivial surface states of samarium hexaboride at the (111) surface. *Nat. Commun.* **10**, 2298 (2019).
The first direct observation of spin-textured surface states for a SmB_6 surface other than the natural (100) cleavage plane.
137. Xu, N. et al. Spin- and angle-resolved photoemission on the topological Kondo insulator candidate: SmB_6. *J. Phys. Condens. Matter* **28**, 363001 (2016).
138. Allen, J. W. Foreward for special issue of philosophical magazine on: topological correlated insulators and SmB_6. *Philos. Mag.* **96**, 3227–3238 (2016).
139. Allen, J. W. Corrigendum for Foreword for special issue of philosophical magazine on: topological correlated insulators and SmB_6. *Philos. Mag.* **97**, 612 (2017).
140. Ishizawa, Y. et al. de Haas-van Alphen effect and Fermi surface of LaB_6. *J. Phys. Soc. Jpn* **42**, 112–118 (1977).
141. Martin, R. M. et al. in *Valence Fluctuations in Solids* Vol. 85 (eds Falicov, L. M. et al.) (North Holland, 1981).
142. Alexandrov, V. et al. Kondo breakdown in topological Kondo insulators. *Phys. Rev. Lett.* **114**, 177202 (2015).
143. Dil, J. H. Spin and angle resolved photoemission on non-magnetic low-dimensional systems. *J. Phys. Condens. Matter* **21**, 403001 (2009).
144. Heinzmann, U. et al. Spin–orbit-induced photoelectron spin polarization in angle-resolved photoemission from both atomic and condensed matter targets. *J. Phys. Condens. Matter* **24**, 173001 (2012).
145. Xu, N. et al. Surface vs bulk electronic structures of a moderately correlated topological insulator YbB_6 revealed by ARPES. Preprint at *arXiv* https://arxiv.org/abs/1405.0165 (2014).
146. Kang, C.-J. et al. Electronic structure of YbB_6: is it a topological insulator or not? *Phys. Rev. Lett.* **116**, 116401 (2016).
147. Xiang, Z. et al. Bulk rotational symmetry breaking in Kondo insulator SmB_6. *Phys. Rev. X* **7**, 031054 (2017).
148. Phelan, W. A. et al. Correlation between bulk thermodynamic measurements and the low-temperature-resistance plateau in SmB_6. *Phys. Rev. X* **4**, 031012 (2014).
149. Xu, Y. et al. Bulk Fermi surface of charge-neutral excitations in SmB_6 or not: a heat-transport study. *Phys. Rev. Lett.* **116**, 246403 (2016).
150. Boulanger, M. E. et al. Field-dependent heat transport in the Kondo insulator SmB_6: Phonons scattered by magnetic impurities. *Phys. Rev. B* **97**, 245141 (2018).
151. Schlottmann, P. NMR relaxation in the topological Kondo insulator SmB_6. *Phys. Rev. B* **90**, 165127 (2014).
152. Valentine, M. E. et al. Breakdown of the Kondo insulating state in SmB_6 by introducing Sm vacancies. *Phys. Rev. B* **94**, 075102 (2016).
153. Xiang, Z. et al. Quantum oscillations of electrical resistivity in an insulator. *Science* **362**, 65–69 (2018).
154. Sato, Y. et al. Unconventional thermal metallic state of charge-neutral fermions in an insulator. *Nat. Phys.* **15**, 954–959 (2019).
155. Stevens, K. W. H. The low lying states of intermediate-valence SmS. *J. Phys. C Solid State Phys.* **13**, L539 (1980).
156. Martin, R. M. Fermi-surfae sum rule and its consequences for periodic Kondo and mixed-valence systems. *Phys. Rev. Lett.* **48**, 362 (1982).
157. Geldenhuys, J. et al. The Luttinger theorem and intermediate valence. *J. Phys. C Solid State Phys.* **15**, 221 (1982).
158. Kaplan, T. A. et al. Theory of the phase diagram in the p-T plane of SmS. *J. Phys. C Solid State Phys.* **12**, L23 (1979).
159. Kikoin, K. A. et al. Magnetic excitations in intermediate-valence semiconductors with a singlet ground state. *J. Phys. Condens. Matter* **7**, 307 (1995).
160. Curnoe, S. et al. 4Electron self-trapping in intermediate-valent SmB_6. *Phys. Rev. B* **61**, 15714 (2000).
161. Abele, M. et al. Topological nonmagnetic impurity states in topological Kondo insulators. *Phys. Rev. B* **101**, 094101 (2020).
162. Park, W. K. et al. Topological surface states interacting with bulk excitations in the Kondo insulator SmB_6 revealed via planar tunneling spectroscopy. *Proc. Natl Acad. Sci. USA* **113**, 6599–6604 (2016).
163. Thomas, S. M. et al. Quantum oscillations in flux-grown SmB_6 with embedded aluminum. *Phys. Rev. Lett.* **122**, 166401 (2019).
164. Aeppli, G. et al. Comments. *Condens. Matter Phys.* **16**, 155 (1992).
165. Hagiwara, K. et al. Surface Kondo effect and non-trivial metallic state of the Kondo insulator YbB_{12}. *Nat. Commun.* **7**, 12690 (2016).
166. Chang, P.-Y. et al. Parity-violating hybridization in heavy Weyl semimetals. *Phys. Rev. B* **97**, 155134 (2018).
167. Fang, Y. et al. Evidence for a conducting surface ground state in high-quality single crystalline FeSi. *Proc. Natl Acad. Sci. USA* **115**, 8558–8562 (2018).
168. Xu, K.-J. et al. Metallic surface states in a correlated d-electron topological Kondo insulator candidate $FeSb_2$. *Proc. Natl Acad. Sci. USA* https://doi.org/10.1073/pnas.2002361117 (2020).
169. Petrovic, C. et al. Kondo insulator description of spin state transition in $FeSb_2$. *Phys. Rev. B* **72**, 045103 (2005).

Acknowledgements
L.L. thanks the NSF (award no. DMR-1707620 for high-field electrical transport) and the DOE (award no. DE-SC0020184 for high-field magnetometry), and K.S. thanks the NSF (award no. NSF-EFMA-1741618 for theory) for supporting this work. All authors thank P.F.S. Rosa and Z. Fisk for illuminating discussions and P. Coleman for sharing his valuable suggestions on the demagnetization effect in isotropic paramagnets. All authors, especially J.W.A., thank J.D. Denlinger for generously sharing his extensive knowledge of SmB_6 ARPES studies.

Author contributions
All authors have read, discussed and contributed to the writing of the manuscript.

Competing interests
The authors declare no competing interests.

Peer review information
Nature Reviews Physics thanks Piers Coleman, Karol Flachbart and the other, anonymous, reviewer(s) for their contribution to the peer review of this work.

Supplementary information
Supplementary information is available for this paper at https://doi.org/10.1038/s42254-020-0210-8.